JAERI-M
86-099

PARAMETRIC STUDY OF FER FIRST WALL AND DIVERTOR PLATE PERFORMANCE

July 1986

John R. HAINES*, Kazunori KITAMURA**,
Takeshi KOBAYASHI and Hiromasa IIDA

日本原子力研究所
Japan Atomic Energy Research Institute

JAERI Mレポートは，日本原子力研究所が不定期に公刊している研究報告書です。
入手の問合わせは，日本原子力研究所技術情報部情報資料課（〒319－11茨城県那珂郡東海村）あて，お申しこしください。なお，このほかに財団法人原子力弘済会資料センター（〒319-11茨城県那珂郡東海村日本原子力研究所内）で複写による実費頒布をおこなっております。

JAERI-M reports are issued irregularly.
Inquiries about availability of the reports should be addressed to Information Division, Department of Technical Information, Japan Atomic Energy Research Institute, Tokai-mura, Naka-gun, Ibaraki-ken 319-11, Japan.

編集兼発行　日本原子力研究所
印　　刷　日立高速印刷株式会社

JAERI-M 86-099

Parametric Study of FER First Wall and Divertor Plate Performance

John R. HAINES*, Kazunori KITAMURA**, Takeshi KOBAYASHI and Hiromasa IIDA

Department of Large Tokamak Research
Naka Fusion Research Estsblishment
Japan Atomic Energy Research Institute
Naka-machi, Naka-gun, Ibaraki-ken

(Received June 13, 1986)

Thermal, mechanical, and lifetime performance of various first wall and divertor plate materials were examined over a broad range of conditions, representative of those considered for next-generation tokamaks such as FER. Candidate plasma side materials include beryllium, graphite, silicon carbide, molybdenum, tantalum, and tungsten. Copper, copper alloy C17510, austenitic stainless steel (316SS), ferritic stainless steel (HT-9), vanadium alloy V-15Cr-5Ti, and molybdenum alloy TZM were considered as candidate heat sink/structural materials. Performance was examined at heat fluxes ranging from 0.05 MW/m^2 for the first wall up to 5.0 MW/m^2 for the divertor plate. Ion flux, plasma edge temperature, burn time per pulse, and number of operating cycles were the other major parameters varied in this study. The analysis model used for these studies includes: (1) a thermal model; (2) a thermal stress model; (3) a disruption erosion model; (4) a sputtering erosion model; and (5) a fatique lifetime model. Results show that recommended first wall and divertor plate designs perform adequately over most of the range of conditions considered for FER design options. Thermal shock of the plasma facing material during intense disruption heating and radiation damage and temperature limitations for graphite are identified as major concerns reguiring experimental investigation.

---

* On assignment by McDonnell Douglas Astronauties Co. from Oak Ridge National Laboratory pursuant to the USDOE/JAERI Agreement on Cooperation in Fusion Research and Development.

** On leave from Toshiba corp.

Keywords: Fusion Experimental Reactor, First Wall, Divertor, Erosion, Fatigue, Plasma Disruption, Thermal Shock, Sputtering, Tungsten, Stainless Steel, Graphite, Copper, Vanadium, Molybdenum, Thermal Stress

核融合実験炉ＦＥＲ第１壁，ダイバータ板特性に関するパラメータ・サーベイ

日本原子力研究所那珂研究所臨界プラズマ研究部
ジョン・ヘインズ* ・喜多村和憲** ・小林　武司・飯田　浩正

（１９８６年６月１３日受理）

ＦＥＲの様な次期大型トカマク装置に於いて想定される，かなり広い範囲の設計条件に於いて，第１壁及びダイバータ板の材料を種々変えてその熱的・機械的及び寿命に関する特性を調べた。プラズマ側のアーマー材としては，ベリリウム，グラファイト，シリコンカーバイト，モリブデン，タンタル，及びタングステンを考えた。また冷却管としては銅，銅合金Ｃ17510，オーステナイト鋼（316ＳＳ），フュライト鋼（ＨＴ－９），バナジウム合金Ｖ－15Cr－５Ti 及びモリブデン合金ＴＺＭを考えた。特性評価を行った熱流束は第１壁に対する 0.05 ＭＷ／m^2からダイバータ板に対する５ＭＷ／m^2までの範囲とした。また入射イオン束，プラズマ・エッジ温度，燃焼パルス幅，運転サイクル数も変数パラメータとして扱った。本検討で取り扱った解析モデルは，(1)熱計算モデル，(2)熱応力計算モデル，(3)プラズマ・ディスラプションによる損耗計算モデル，(4)スパッタリング損耗計算モデル，(5)疲労寿命計算モデルである。

解析の結果に基き，想定される負荷条件範囲（熱流束，プラズマエッジ温度）に応じて最適組合せを提案した。これらはＦＥＲで想定される設計条件の大部分で充分な特性を有することが分った。また今後実験による検討を要すると思われる重要な事項として，プラズマ・ディスラプション中の極めて大きな熱負荷に於ける，アーマ材の熱衝撃，中性子による放射線損傷，及びグラファイトの許容温度である事を指摘した。

那珂研究所：〒３１１－０２　茨城県那珂郡那珂町大字向山８０１－１

＊　マクダネル・ダグラス社からオークリッジ研究所へ出向中のところ
核融合開発に関するＪＡＥＲＩ／ＵＳＤＯＥ関の協定によりオークリッジ研究所より日本原子力研究所に派遣された。

＊＊　外来研究員（東芝）

Contents

目　　次

1. INTRODUCTION

Performance of the first wall and divertor plate in future experimental reactors, such as the Fusion Experimental Reactor (FER), is a critical design issue receiving considerable attention in recent experimental and analytical studies. The lifetime of these components, which are subjected to intense heating conditions and bombardment by high energy particles, is the major design issue. Three mechanisms potentially limit the lifetime of these components. These mechanisms are:

(1) Thermal stress fatigue due to pulsed heating during the burn phase as well as during plasma disruptions.

(2) Erosion of the surface material by energetic particle sputtering or by melting and vaporization during intense plasma disruption heating.

(3) Radiation damage to the materials by high energy neutrons leading to swelling, creep, and property changes.

As pointed out in previous studies[1], the plasma edge conditions have a dramatic effect on first wall and divertor plate design and lifetime performance. This study seeks to establish first wall and divertor plate thermal, mechanical, and erosion performance over a broad range of plasma edge conditions. Both normal operating and disruption conditions are examined to establish the thermal stress fatigue and erosion lifetimes for various material candidates. Radiation damage effects are neglected in this study, except for the special case of low fluence damage of graphite. The purpose of this study is to identify the most promising material and configuration features for specific ranges of operating conditions.

Past studies of a similar nature, either neglected the effects of disruptions[2-6], or evaluated the thermal stresses caused by intense disruption heating for a specific material and design configuration using sophisticated elastic-plastic analysis models. In this study, the disruption heating effects are included by using a simple elastic-plastic analysis procedure that facilitates the examination of component performance in a parametric fashion.

Details of the operating conditions, material and design options, and analysis methods used in this study compose the subsequent sections of this report. Recommendations concerning materials and

design features are discussed in the section following performance results. Finally, issues that require resolution to achieve a reasonable level of confidence in the viability of designing first wall and divertor plate components for FER and a brief set of concluding remarks are presented.

2. ANALYSIS CONDITIONS AND ASSUMPTIONS

Conditions defined to reflect several options of the FER design are listed in Table 1. Cases 1 and 2 of Table 1 represent first wall design conditions, whereas Cases 3 through 6 represent divertor plate or limiter design conditions. Cases 1 and 2 are distinguished by the first wall heat flux during plasma disruptions. For Case 1, peak energy densities ranging from 0.6 to 1.2 MJ/m^2 are considered. Peak disruption energy densities up to 5.0 MJ/m^2 are included in Case 2. The remaining first wall design conditions are the same for Cases 1 and 2.

The divertor plate cases reflect different plasma edge conditions for the burn and recharge phases of the operating cycle. Case 3 represents a burn phase with high radiation power loss, whereas Case 4 represents low radiation loss conditions. Case 3' represents a recharge phase with low edge temperature and Case 5 a high edge temperature recharge phase. Case 6 defines the range of conditions expected for a pumped limiter.

The two sets of burn phase and recharge phase conditions defined for the divertor plate are combined to form the four sets of operating options for the divertor defined in Table 2. Option 1 combines the high radiation power loss burn phase (Case 3) with the low edge temperature recharge phase (Case 3'). This option is essentially the same as the reference conditions for the FY 85 version of FER.

Using the information shown in Table 1, the overall range of conditions to be examined in this study are defined in Table 3 for the divertor plate and Table 4 for the first wall. Considering the full range of parameters listed in Tables 3 and 4, analyses were performed and results are presented in a parametric fashion in section 5 of this report. To translate these parametric results into information useful for FER design studies, the recommendations discused in section 6.0 refer to the case and options defined in Tables 1 and 2.

Divertor plate heat fluxes during normal operation range from 1.0 to 5.0 MW/m^2, and the disruption energy density striking the divertor during the 5 ms thermal quench phase of the disruption ranges from 1.5 to 3.0 MJ/m^2. For the first wall, heat fluxes up to 0.5 MW/m^2 were considered for normal operation. Energy densities up to 5.0 MJ/m^2 striking the first wall during the current quench phase of the

disruption were studied.

Sputtering erosion of the divertor plate was evaluated for plasma edge temperatures ranging from 5 to 300 eV. The peak particle flux was assumed to be inversely proportional to the plasma edge temperature, i.e. constant transport power to the divertor. A peak particle flux of 5×10^{22} $m^{-2} \cdot s^{-1}$ is assumed as the reference value at an edge temperature of 20 eV. First wall sputtering by charge exchange neutral particles is expected. The flux of particles is assumed to be 1.8×10^{22} $m^{-2} \cdot s^{-1}$ and the energy of the particles was varied from 60 eV to 200 eV in these studies.

The burn time per pulse was varied from 30 s to 2000 s and the total number of burn pulses was assumed to be in the range of 10^3 to 10^5. Neutron fluences equivalent to up to 0.3 MW·yr/m^2 of 14 MeV fusion sourse neutrons were considered. At these relatively low fluences, radiation damage effects should be minimal for most materials, except graphite, considered in this study. The effects of radiation damage on graphite performance are discussed in later sections of this report.

Key analysis assumptions are listed in Table 5. A nominal water coolant bulk temperature of 40 °C is assumed, which is consistent with the use of conventional heat exchanger and cooling tower equipment. Heat transfer coefficients of 10 kW/m^2·K for the first wall and 25 kW/m^2·K for the divertor plate are assumed. These values are well within the capability of high performance coolant channel design and performance. A neutron wall loading of 0.88 MW/m^2, the reference value for FER in FY '84 (slightly higher than the 0.68 MW/m^2 value for the FY '85 reference design) was used. Radiation heat transfer from the surface facing the plasma can be significant with some of the materials and design configurations studied. An area view factor of 0.5 to a surface at a temperature of 300 °C is assumed. This represents radiation to an actively cooled first wall. The inboard wall may have high temperature armor, and thus may not be a significant radiation heat sink for the divertor.

The mixture of ions leaving the plasma is assumed to be composed of 46.5 % deuterium, 46.5 % tritium, 1 % protons, 5 % helium ash, and 1 % oxygen impurity during the burn phase, and 45 % deuterium, 45 % tritium, and 10 % oxygen impurity during the recharge phase. The charge states of impurity ions and previously sputtered material returning to the divertor are assumed to be 2 and 4, respectively.

3. MATERIAL AND DESIGN OPTIONS

Bare metal as well as duplex armor and heat sink structures were considered for the first wall and divertor plate design. Structural heat sink material candidates included OFHC-Copper, copper alloy C17510, molybdenum alloy TZM, and vanadium alloy V-15Cr-5Ti for the divertor plate, and austenitic stainless steel 316SS, ferritic stainless steel HT9, vanadium alloy V-15Cr-5Ti, and molybdenum alloy TZM for the first wall. Armor material candidates for the divertor plate are beryllium, graphite, silicon carbide, molybdenum alloy TZM, and tungsten. Graphite, silicon carbide, and beryllium were evaluated as potential first wall armor materials. Material properties used for this study are discussed in Appendix A.

Performance of several types of armor to heat sink attachment concepts was examined. Radiation cooling of the armor, representative of mechanically attached armor tiles, was considered for use at first wall type heat fluxes with graphite or silicon carbide armor. The temperature of radiation cooled armor is excessively high at divertor plate type heat fluxes. Direct bonding (eg. brazed or diffusion bonded) attachments were evaluated for both components. The thermal contact resistance of the bond was assumed to be negligible for this type of attachment. The use of an intermediate layer of material between the armor and heat sink was also examined. For the divertor plate, performance of a copper plated graphite fiber matrix concept developed by Hitachi was evaluated[7]. Although the properties of this matrix material can be adjusted by changing the ratio of graphite to copper content, only the single set of representative properties shown in Table 6 were used in this study. The thermal conductivity of this material is quite high, thus making this concept attractive for use in the divertor plate design.

The Brunsbond H-875 metal fiber compliant layer[8] was considered for use in attaching the first wall armor to the cooled structure. Properties of this compliant layer are controlled by density. The density is chosen to achieve a balance between compliance, thermal conductivity, and strength. A 35 % dense matrix was considered in this study because the properties of this design, shown in Table 6, were available. Because of its relatively low thermal conductivity, this concept cannot be considered for the divertor plate design.

4. ANALYSIS METHOD

The analysis model used for these studies includes: (1) a one-dimensional, transient thermal model; (2) a disruption melting and vaporization erosion model; (3) a one-dimensional, simple elastic-plastic thermal stress model; (4) a sputtering erosion model; and (5) a fatigue lifetime model. Details of the thermal model, including the melting and vaporization model, and the thermal stress model are described in Appendix B.

The one-dimensional finite difference thermal model includes heat input by surface heating as well as by bulk neutronic heating. Temperature dependent thermal properties are used for determining the heat diffusion through the divertor plate or first wall structure. Radiation heat transfer from the heated surface to other surfaces inside the reactor and convection heat transfer to the water coolant are also considered in the model.

The disruption erosion model accounts for the energy absorbed by vaporization and melting, that may be caused by the intense disruption heating. Thus, erosion by these mechanisms and the impact of the phase change energy sinks on the resulting transient temperature and thermal stress distribution are predicted.

Thermal stresses are calculated in the one-dimensional plate assuming that the plate is allowed to expand but constrained from bending. Temperature dependent physical properties are used to calculate the elastic stress and strain distribution through the plate. Equivalent plastic strains are determined using the simple elastic-plastic model described in the ASME Boiler and Pressure Vessel Code (ASME BPV-III-1-NB). These equivalent plastic strains are used to evaluate the fatigue lifetime. Except for the study concerned with the effects of irradiation on IG-110 graphite, the calculated or design fatigue lifetimes as prescribed in the ASME Code include a factor of 20 reduction in cycles or a factor of 2 increase in strain to failure, whichever is more limiting.

Irradiation damage to graphite may be significant at the fluences considered in this study. To examine the potential impact of irradiation damage at relatively low fluences, data for irradiated IG-110 graphite were used in this study. Analyses results are also presented for GRAPHNOL-N3M and IG-110 in the unirradiated condition. The results

for unirradiated graphite are expected to apply for fluences less than about 0.01 MW yr/m^2. Although other types of graphite, such as GRAPHNOL-N3M are likely to be superior to IG-110 in applications to first walls of fusion devices a significant irradiation effect database exists for IG-110 (and not for GRAPHNOL-N3M) because of its application in the Japanese High Temperature Gas-Cooled Reactor (HTGR) program. The isotropic IG-110 graphite is not optimized with respect to thermal shock or thermal stress cabability. Therefore, some improvements in the irradiation performance of graphite presented in this study should be possible through development of a more extensive database.

For the study of IG-110 graphite performance, the fatigue lifetime guidelines used in the HTGR program are used in this study. These guidelines specify that the fatigue lifetime for graphite used as support structure of reactor components should be reduced by a factor of 3 below experimental data. The data used for this guideline is that corresponding to survival of 99 % of the test specimens with a 95 % confidence level. Fatigue data for irradiated graphite is quite sparse, but, in general, the fatigue stress limit increases with irradiation. Since the elastic modulus increases with irradiation by about the same ratio or greater, the strain to failure likely decreases slightly. It is mentioned in Ref. 11, that the fatigue stress limit for H-451 graphite increases as the square root of the increase in the elastic modulus. This implies that the strain to failure decreases by the square root of the increase in the elastic modulus. In the HTGR program guidelines, part of the rationale used in selecting the reduction in lifetime cycles by a factor of three below the unirradiated data is to allow for irradiation effects. Thus, unirradiated fatigue data are used for the analysis; i.e. irradiated fatigue data should not be used since the reduction in fatigue life is already accounted for in the guideline. Irradiation effects on other properties, such as thermal conductivity, elastic modulus, and expansion coefficient are included in this analysis.

Sputtering yields are determined using the model and data of Ref. 12. Sputtering by previously sputtered material (self sputtering) is included. The peak net sputtered material Γ_s is given by:

$$\Gamma_s \leq \Gamma_p \cdot \frac{1}{1 - y_s(e_s)} \sum y_{pi}(e_i) f_i$$

where $y_{pi}(e_i)$ = the sputtering yield of plasma species i at energy e_i
f_i = the fractional content of species i in the plasma
Γ_p = the peak flux of plasma particles striking the surface
$y_s(e_s)$ = the self sputtering yield at energy e_s

Redeposition of sputtered material is not included in this simple model. Also, all sputtered material is allowed to return to cause self sputtering. Therefore, the sputtering erosion rate calculated with this simple model should be interpreted as an upper limit.

Self sputtering yields are shown in Figure 1 as a function of plasma edge temperature. The charge state of these ions is assumed to be four. Thus, the energy of the ions striking the divertor plate is:

$$E = \frac{3}{2} kT_e + 4\phi kT_e = 13.5\ kT_e$$

where k is Boltzmann's constant, T_e is the plasma edge temperature, and ϕ is the sheath factor (assumed to be 3 in this case). The self sputtering yields for tungsten, molybdenum, and SiC exceed unity at edge temperatures of about 45 eV, 55 eV, and 100 eV, respectively. This results in an unstable situation leading to excessive contamination and quenching of the plasma. Self sputtering for graphite and beryllium remain below unity for all edge temperatures.

Chemical sputtering erosion and sputtering by radiation enhanced sublimation of graphite are not included. Based on reviews of chemical erosion data[13,14] and on recent experience with graphite armor in current generation tokamaks like TFTR, there is evidence that these erosion mechanisms are not significant in tokamak environments. Further discussion of graphite temperature limitations is presented in subsequent sections of this report.

A flow diagram for the computer code used in these studies is shown in Figure 2. Input conditions include the geometry information, material properties, and normal operating and disruption conditions. The thermal and structural analyses for normal operating conditions are carried out at each time step. After reaching the end of the burn phase these temperatures are used as intial values for the disruption analysis. The stress/strain ranges are then used to compute the fatigue lifetime,

i.e. number of cycles, for normal operating pulses as well as disruptions. Erosion by melting and vaporization during disruptions are computed along with the sputtering erosion to determine the erosion lifetime. The code has the capability to solve the coupled erosion/fatigue lifetime problem. However, because the erosion predictions are subject to large uncertainties, results for the decoupled case only are reported here. In most cases, the fatigue lifetime is improved as erosion occurs since the temperatures and stresses are decreased. Thus, the decoupled solution should be somewhat conservative. The final output from the computer code lists:

(1) temperature distributions
(2) stress and strain distributions
(3) end-of-life based on fatigue
(4) end-of-life based on erosion.

5. ANALYTICAL PERFORMANCE

5.1 Divertor PLATE Performance

Fatigue lifetime performance for disruption and normal operating conditions was examined for all combinations of armor and heat sink materials at a nominal set of heating conditions (1.5 MW/m^2 surface heat flux during normal operation and 2.4 MJ/m^2 peak energy density during the 5 ms duration thermal quench). After these initial studies, the combinations of materials were narrowed to those shown in Table 7. Initial studies also indicated that providing an armor thickness of roughly 10 mm adequately protects the heat sink material from plasma disruption heating, while limiting temperatures and thermal stresses to reasonable levels during normal operation and providing a significant thickness of material for erosion lifetime purposes. Thus, an armor thickness of 10 mm was used for the remaining studies which examined the performance of the selected materials over the broad range of divertor plate conditions. Performance parameters reported in this study could, in general, be further optimized with respect to armor thickness.

5.1.1 Normal Operating Performance

Fatigue lifetime performance for the selected divertor plate material combinations are shown in Figure 3 for normal operating heat fluxes up to 5.0 MW/m^2. The combination of tungsten armor with the high strength copper alloy C17510 heat sink has the best fatigue performance. A divertor plate constructed of molybdenum alloy TZM armor and a vanadium alloy V-15Cr-5Ti heat sink also has good performance. Graphite (unirradiated GRAPHNOL-N3M) attached to an OFHC copper heat sink has the best fatigue performance of the material candidates containing a low atomic number armor material. Beryllium stresses are quite high for the 10 mm thick armor at the higher heat fluxes. Fatigue performance limits its usage to heat fluxes below about 1.8 MW/m^2.

5.1.2 Disruption Performance

Fatigue performance of the heat sink materials for disruption conditions is shown in Figure 4. As indicated above, using a 10 mm thick armor leads to reasonably good performance over the entire range of disruption conditions. For the armor materials, compressive stresses near the heated surface of the armor exceed ultimate strength values

for all materials except tungsten and possibly some grades of graphite. The damage caused by these thermal shock conditions is not clear. Thus, thermal shock testing must be included as a vital part of the program to develop a viable divertor plate design.

5.1.3 Irradiation Damage Effects for Graphite

Peak temperatures and thermal stresses calculated for IG-110 graphite in the unirradiated and irradiated conditions (3×10^{25} n/m^2 fluence) are shown in Figures 5 and 6 for direct bonding and intermediate layer attachment concepts. As the fatigue lifetime limits indicated in these two figures show, the performance for the intermediate layer concept is significantly better than that for the direct bonding concept. Using a fatigue limit of 10^4 cycles, the heat flux is limited to be less than 2.6 MW/m^2 for unirradiated IG-110 graphite and 1.3 MW/m^2 for IG-110 irradiated to 3.0×10^{25} n/m^2. The fatigue/irradiation damage interaction was examined by coupling the two processes in the computer code. Fatigue damage was calculated for an incremental increase in operating cycles with properties interpolated linearly on a logarithmic scale with neutron fluence. Unirradiated data were assumed to correspond to fluences below 10^{24} n/m^2. Fatigue lifetime dependence on heat flux and burn pulse duration are shown in Figure 7. At the longest burn time studied here (2000 seconds), a fatigue lifetime of 10^4 cycles is possible at heat fluxes up to 1.3 MW/m^2 using the intermediate layer concept. If the burn duration is reduced to 200 seconds, the heat flux limit is increased to 2.2 MW/m^2. It is hoped that these relatively low limits on the heat flux can be increased considerably by using a grade of graphite more suitable for high thermal stress applications.

5.1.4 Erosion Performance

Predicted vaporization and melting erosion of the armor caused by plasma disruptions is shown in Figure 8. Tungsten and graphite perform extremely well over the entire range of conditions. A relatively thick melt layer and significant vaporization occurs with beryllium armor. Also, a thick layer of dissociated silicon carbide is formed during disruptions.

Sputtering erosion lifetimes for all armor material candidates are shown in Figure 9 as a function of plasma edge temperature. As

mentioned previously, redeposition is not included in determining the sputtering erosion lifetime. For tungsten, sputtering erosion at the nominal edge temperature of 20 eV is quite low. However, as the edge temperature approaches about 40 eV, the self sputtering yield of tungsten approaches unity. Above about 45 eV, tungsten armor cannot be used. Self sputtering for molybdenum and silicon carbide is predicted to exceed unity at edge temperatures of 55 eV and 110 eV, respectively. Self sputtering for the low-atomic number materials, beryllium and graphite, does not exceed unity at any edge temperature. From the sputtering erosion curves shown in Figure 9, we conclude that tungsten has the best performance for edge temperatures below 40 eV, molybdenum has the best performance between 40 eV and 50 eV, graphite has the best performance between 50 eV and 220 eV and beryllium has the best performance at edge temperatures above 220 eV.

Using these "optimum" materials in the edge temperature ranges specified above, a design for providing 10^3-200 second burn cycles is possible at all edge temperatures. Designs to last 10^4-200 second burn cycles cannot be provided if the edge temperature is between 40 eV and 230 eV. Designs can not be expected to last 10^5-200 second burn cycles at edge temperatures between 22 eV and 680 eV.

Knowing the edge temperature within a relatively small uncertainty before operating FER is a prerequisite to providing the optimum design. In the worst but yet plausible case, if we cannot insure that the edge temperature is below about 50 eV, we must provide a low-atomic number armor material that will avoid self sputtering run away. If the edge temperature is then found to be low, say 20 eV, the sputtering erosion lifetime may be very short (predicted to be about 500-2000 second cycles for graphite with no redeposition) in comparison to the "optimized" material (tungsten) lifetime of 10^4-2000 second cycles at 20 eV.

5.1.5 Performance for FER Operating Options

Performance at nominal conditions for each of the four divertor plate options are shown in Table 8 through 11. These tables list the armor and heat sink material fatigue lifetimes and erosion lifetime based on normal operating and disruption conditions. As shown in these tables, the number of normal operating cycles is usually controlled by sputtering erosion. This is somethat misleading because redeposition

of the sputtered material should significantly increase the lifetime[10]. Thus, comparisons between the sputtering erosion lifetimes and fatigue lifetimes calculated in this study are difficult. However, comparisons of the sputtering erosion lifetimes between two different armor materials should be qualitatively correct.

The other remarkable feature shown in these tables is the very low disruption fatigue lifetimes for the armor materials. Thermal shock of the armor, on the first disruption event is expected for all armors except tungsten and perhaps graphite. Damage to tungsten and graphite may occur after a relatively low number of disruption cycles. The extent or implications of this damage is not clear. There is some evidence that because of the highly localized nature of the stresses only a thin layer of material flakes off of the heated surface. Further experimental studies of this type of process are reguired to understand the impact of this damage on the structural integrity of these types of duplex structures.

Recommendations based on the performance results presented in Tables 8 through 11 are presented in section 6 of this report.

5.2 First Wall Performance

Several types of first wall designs were evaluated. The simplest design is a bare metal structure. Attaching armor tiles to a metallic heat sink structure adds significant complexity to the first wall design. The armor could be attached by mechanical means (radiation cooled), by bonding directly to the heat sink, or by bonding to an intermediate compliant layer material which is bonded to the heat sink. The advantages and limitations of each type of design are listed in a qualitative fashion in Table 12. Some of the limitations listed in this table will be discussed quantitatively in the following paragraphs.

5.2.1 Bare Metal Design Concepts

The major limitation of the bare metal design is the susceptability of damage to the primary coolant structure during plasma disruption events. Fatigue and erosion lifetime limits caused by disruption heating are shown in Figures 10 a and 10 b for the four structural materials considered as first wall candidates. The fatigue limits are more restrictive than the disruption erosion limits. For a heating duration

of 15 ms, the energy density limitation based on a fatigue lifetime of 100 disruptions is 0.21 MJ/m^2 for 316SS, 0.4 MJ/m^2 for HT9, 0.7 MJ/m^2 for V-15Cr-5Ti, and 0.95 MJ/m^2 for Mo alloy-TZM. The nominal first wall energy density expected during disruptions in FER is 1.2 MJ/m^2.

5.2.2 Radiation Cooled Design Concepts

Thermal performance analysis results for a radiation cooled inboard wall constructed of graphite or silicon carbide armor are shown in Figures 11 and 12. Fatigue performance should be less restrictive than temperature limitations for the radiation cooled design concept. Using a 1000 °C temperature limit for graphite, based on excessive erosion by radiation enhanced sublimation, a heat flux of 0.25 MW/m^2 is acceptable if the burn duration is less than 40 seconds (250 second dwell time between burns assumed). For burn durations greater than 200 seconds, the heat flux limit is less than 0.02 MW/m^2. If the graphite temperature limit is set at 2000 °C, based on excessive sublimation, the heat flux limit for a steady state burn is 0.9 MW/m^2.

Using radiation cooled silicon carbide armor with a temperature limit of 1440 °C, based on excessive sublimation, the nominal heat flux of 0.25 MW/m^2 can be withstood for burn durations up to 80 seconds. However, the heat flux is limited to only 0.05 MW/m^2 for burn durations greater than 500 seconds.

The effect of using armor on the entire inboard and outboard first wall, thus eliminating radiation cooling from the plasma side surface, is shown in Figure 13. At the nominal first wall heat flux of 0.25 MW/m^2, the peak surface temperature for 30 mm thick armor tiles covering the entire first wall is about 1900 °C, which is almost 400 °C hotter than for the design with inboard armor only. Allowing the graphite to operate at a temperature of 2000 °C, the maximum heat flux that can be tolerated is 0.3 MW/m^2. This compares with a heat flux limit of 0.9 MW/m^2 for the design with armor on the inboard wall only.

The effect of irradiation damage to graphite was also studied for the radiation cooled consept. Since heat transfer by radiation is the controlling mechanism, the temperatures were only slightly increased (e.g. about 50 °C hotter for the nominal heat flux of 0.25 MW/m^2). Therefore, the limits on heat flux for radiation cooled graphite are essentially unaffected by irradiation damage.

5.2.3 Bonded Attachment Design Concepts

All armor and heat sink material combinations with a bonded or compliant layer design have adequate lifetime performance for normal operation at the nominal heat flux of 0.25 MW/m^2. The major advantage of using a bonded armor design is the potential to maintain the temperature of graphite below about 400 °C, thus avoiding chemical erosion concerns, or for the case of beryllium armor, maintaining temperatures below limits for loss of material by sublimation. Graphite armor has better fatigue and disruption erosion performance than beryllium and thus, attention was given to establishing the graphite armor limits for bonded attachment concepts.

Maximum graphite armor temperatures are shown in Figure 14 for designs using direct bonding or an intermediate compliant layer between the armor and heat sink. For a 10 mm thick graphite armor thickness directly bonded to a 316SS heat sink the graphite temperature remains below 400 °C for heat fluxes up to 0.85 MW/m^2. If a Brunsbond Pad compliant layer is used, the heat flux must be limited to 0.48 MW/m^2 or below to maintain the graphite temperature below 400 °C.

The bonded or compliant layer concept can, of course, be used beyond the limits discussed above, however, the surface temperature will exceed 400 °C. Fatigue limitations as a function of heat flux are presented in Figure 15 for graphite armor attached to 316SS. For a fatigue lifetime of 10^4 normal operating cycles, the heat flux must be maintained below 0.58 MW/m^2 for direct bonding or 0.80 MW/m^2 with a compliant layer design (316SS fatigue limits lifetime in this case).

The effect of irradiation damage on graphite armor performance for bonded attachments is summarized in Figures 16 through 18. The maximum temperature for IG-110 graphite in the unirradiated and irradiated conditions are plotted in Figure 16 for direct bonding and compliant layer concepts. Temperatures for unirradiated GRAPHNOL-N3M graphite are shown in this figure for comparison. Using a 400 °C limit to avoid chemical sputtering concerns, a 10 mm thick IG-110 graphite armor tile irradiated to a fluence 3×10^{25} n/m^2 is limited to heat fluxes below 0.38 MW/m^2 for the direct bonding design concept and 0.29 MW/m^2 for the compliant layer design.

If the chemical erosion concern is neglected, thermal stress fatigue damage concerns will limit the heat flux. Thermal stresses

for IG-110 graphite in the unirradiated and irradiated condition are shown in Figures 17 and 18 for direct bonding and compliant layer designs, respectively. For a fatigue lifetime of 10^4 cycles, the heat flux must be limited to about 0.32 MW/m^2 for the bonded attachment and 0.76 MW/m^2 for the compliant layer design concept. As discussed in previous sections of this report, it is likely that this fatigue performance can be improved by selecting a grade of graphite other than IG-110, such as GRAPHNOL-N3M, that has better thermal stress capabilitics.

5.2.4 Erosion Performance

Disruption melting and vaporization erosion lifetimes for the candidate armor materials are shown in Figure 19 for energy densities up to 5.0 MJ/m^2. A large melt layer for beryllium and a thick layer of dissociated silicon carbide are formed at the higher energy densities. Also, vaporization of beryllium and silicon carbide can be quite large. Graphite experiences negligible erosion by vaporization and no melting over the entire range of energy densities.

Sputtering erosion lifetime performance is shown in Figure 20 for all first wall candidate materials as a function of neutral particle energy. Vanadium has the best sputtering erosion lifetime performance. A 10 mm thick graphite armor tile has a lifetime ranging from about 8×10^5 cumulative burn seconds (4×10^4 -200 s burn pulses) to about 1.4×10^5 cumulative burn seconds per mm of armor thickness. At burn times of a few hundred seconds or less, armor lifetimes should be longer than the FER device lifetime. For example, with a burn time of 200 s and a charge-exchange neutral particle energy of 100 eV, the sputtering erosion lifetime of a 50 mm thick graphite armor tile is expected to be about 10^5 cycles. However, at the nominal FER burn time of 2000 s, a lifetime of about 10^4 cycles is expected. Thus, replacement of first wall components in regions of high neutral particle flux should not be required unless the cumulative burn time is in the high end of the range considered in these studies.

6. RECOMMENDED DESIGN CONCEPTS

6.1 Divertor Plate

A summary of recommended divertor plate design concepts is presented in Table 13. For plasma edge temperatures below 40 eV and heat fluxes below 1.5 MW/m^2 a tungsten armor, OFHC-Copper heat sink design is recommended. For heat fluxes above 1.5 MW/m^2, a copper alloy C17510 heat sink is recommended. A design with molybdenum alloy-TZM armor and a V-15Cr-5Ti heat sink is recommended if the edge temperature is between 40 eV and 50 eV. For edge temperatures above 50 eV graphite armor with an OFHC-Copper heat sink is recommended. Using a compliant layer between the graphite and copper significantly increases the fatigue lifetime and is therefore recommended.

Performance evaluations for graphite including irradiation damage effects suggest that this mechanism may limit the use of graphite in FER to heat fluxes in the range of about 2 MW/m^2. Therefore, for edge temperatures above 50 eV and fluences exceeding about 0.05 MW-yr/m^2, none of the designs/materials studied performed adequately at high heat fluxes. Improvement of the data base of graphite grades with improved thermal stress resistance under irradiation conditions may lead to solutions to this problem.

Graphite is recommended over beryllium as a low-Z armor material because of its superior fatigue lifetime performance during normal operation and disruptions and also because of its superior disruption erosion performance. Erosion of graphite by mechanisms other than physical sputtering, i.e. chemical erosion or radiation enhanced sublimation were not included in these studies. Based on a review of chemical erosion data and on recent experience in operation tokamak devices such as TFTR with large areas of the first wall covered with graphite armor operating at high temperatures, these enhanced erosion effects are assumed to be negligible at reactor type conditions. However, if it is concluded that this assumption is invalid, these recommendations must be reexamined.

Based on the above discussion the recommended designs for each of the four divertor operating options and the pumped limiter design case are listed in Table 14.

6.2 First Wall

Recommended first wall design concepts are summarized in Figures 21 through 24 for each of the four structural heat sink materials. Limits on normal operating heat flux or disruption energy density based on either fatigue lifetime (assuming that the ASME BPV guidelines are adopted) or temperature limits are indicated in each figure. A bare 316 SS first wall is recommended if the energy density during a 50 ms long disruption is below 0.5 MJ/m^2. At energy densities above this value, graphite armor is recommended. The disruption energy density ranges from 0.6 MJ/m^2 to 1.2 MJ/m^2 for Case 1 and 1.2 to 5.0 MJ/m^2 for Case 2 of the FER first wall design conditions defined in Table 1. Therefore, graphite armor is recommended for either FER design case if a 316 SS structure is used. For heat fluxes below 0.9 MW/m^2, a radiation cooled design is recommended assuming that a 2000°C graphite temperature is allowed. If the graphite temperature must be maintained below 400°C to avoid chemical sputtering of if the heat flux exceeds those specified for a radiation cooled design, a bonded attachment concept such as brazing must be used.

Mo-TZM and V-15Cr-5Ti structures have the best fatigue lifetime performance and the fatigue performance of HT9 slightly exceeds that of 316SS. However, it should be noted that at a nominal normal operating heat flux of 0.25 MW/m^2, 316SS performance should be quite adequate. Therefore, unless the bare metal concept is used or the first wall heat flux during normal operation is increased significantly beyond values currently considered for FER, the selection of first wall structural material should be based on criteria other than fatigue performance.

7. ISSUES

There are several key issues for first wall and divertor plate design. Thermal shock damage of all armor materials except tungsten and possibly graphite is expected during disruption heating conditions. If we choose to use any of these materials, testing is required to establish limits beyond which thermal shock damage occurs and we must also understand the impact of this type of damage on the integrity of the design.

For graphite armor, chemical sputtering and enhanced sputtering at temperatures above 1000°C are major concerns. Although these mechanisms are found in laboratory scale experiments, there is little evidence for these phenomena in actual tokamak environments. Understanding this apparent discrepancy is necessary to establish confidence in the viability of a graphite armor design for a next-step device such as FER. Also, radiation damage of graphite may significantly reduce its thermal conductivity, even at low fluence. The degree of reduction depends on the fluence as well as the type or grade of graphite. Development and performance testing of graphite materials that combine the best mix of thermal, structural, and radiation damage resistance properties should be investigated.

At edge temperatures above about 50 eV, a low-Z armor material such as graphite or beryllium must be used. Significant redeposition of sputtered material must occur for these materials to achieve a reasonable erosion lifetime. Although the arguement for expecting significant redeposition is quite convincing, experiments to better understand this mechanism, particularly in actual tokamak environments, are desirable. The properties of redeposited material and the impact of any property changes must also be studied.

Since the structural design criteria significantly influence performance predictions and this could impact design and material selection, development of a criteria for fusion components must be an important part of the R & D program for a next-step device. The ASME Code has been applied in this study because of a lack of another reasonable standard, but this criteria may be overly conservative especially for use in evaluating performance during off-normal disruption events or in determining armor lifetime.

8. Conclusions

A parametric study of divertor plate and first wall performance was carried out to identify promising designs and understand design limitations. Though the direct application of the ASME Code for design evaluation of the divertor and first wall may be conservative, it is temporarily applied as the structural design standard for FER reactor structures because of a lack of other reasonable standards. Recommended designs were shown to perform adequately at nominal conditions for each of the four divertor operation options and two first wall cases that represent possible design parameters for FER. Specific conclusions are listed below:

8.1 Divertor Plate

(1) A design with tungsten armor bonded to a copper alloy (C17510) heat sink has excellent thermal and mechanical performance over the entire range of heat fluxes considered.

(2) Self sputtering yields for tungsten, molybdenum, and SiC armor exceed unity at edge temperatures above 45 eV, 55 eV, and 110 eV, respectively. Self sputtering yields for the low-Z armor materials, graphite and beryllium, remain below unity at all energies.

(3) At high edge temperatures (above about 50 eV), graphite is recommended over beryllium as the armor material because of its superior fatigue lifetime during normal operation and its excellent resistance to thermal shock damage during disruptions.

(4) Fatigue and radiation damage interaction, even at the relatively low fluences planned for FER, may limit the heat flux that can be tolerated using graphite to under 2 MW/m^2. Graphite materials that have better thermal stress and radiation damage performance may already exist but testing is required to establish the irradiation performance of these materials.

(5) None of the material combinations examined performs adequately at the most extreme combination of edge temperature (above 50 eV), heat flux (above 2 MW/m^2), and neutron fluence (above 0.3 $MW\text{-}yr/m^2$).

(6) Thermal shock damage of most armor materials during disruption heating conditons is expected. The impact of this damage on the structural integrity of the armor and the bond layer are critical issues requiring further experimental investigation.

8.2 First Wall

(1) All armor and heat sink material combinations considered in this study have acceptable fatigue performance for the nominal normal operating conditions expected for FER.

(2) A bare metal first wall, with no armor, is adequate if the energy density during disruptions is low enough. These limits are:

Structural Material	Energy Density Limit (MJ/m^2) 15 ms Disruption	50 ms Disruption
316 SS	0.2	0.5
HT-9	0.4	0.85
V-15Cr-5Ti	0.7	1.4
Mo-TZM	0.95	2.2

(3) Radiation cooled graphite armor is recommended for the first wall if the disruption energy flux exceeds the above limits for bare metal walls and if the heat flux during normal operation is low enough. These heat flux limits are:

ARMOR COVERAGE	HEAT FLUX LIMIT (MW/m^2) 1000°C LIMIT	2000°C LIMIT
INBOARD WALL ONLY	0.02	0.9
ENTIRE FIRST WALL	< 0.01	0.3

(4) Graphite bonded with or without a compliant layer to any of the heat sink materials should be used if: (a) the energy density during desruptions exceeds limits for bare metal walls, and (b) either the normal operating heat flux exceeds limits for radiation cooled armor concepts, or operating below about 400°C is judged to be necessary to avoid chemical erosion problems.

(5) Disruption erosion is negligible for graphite armor. Melting and vaporization of bare metal first walls is significant, however fatigue damage provides a more severe limit on disruption energy density.

(6) Sputtering erosion of the first wall in regions of high neutral particle flux is significant. Replacement of first wall components in these regions during the lifetime of the FER may be required, at high values of cumulative burn time.

(7) Thermal shock damage during disruptions and graphite chemical sputtering and radiation enhanced sublimation are the major first wall design issues.

Acknowledgements

The authors would like to thank Y. Sawada, N. Fujisawa, S. Yamamoto, and S. Tsujimura for their valuable guidance and discussions in this study. They also acknowledge Drs. S. Tamura, M. Yoshikawa, and K. Tomabechi for their support and encouragement.

(7) Thermal shock damage during disruptions and graphite chemical sputtering and radiation enhanced sublimation are the major first wall design issues.

Acknowledgements

The authors would like to thank Y. Sawada, N. Fujisawa, S. Yamamoto, and S. Tsujimura for their valuable guidance and discussions in this study. They also acknowledge Drs. S. Tamura, M. Yoshikawa, and K. Tomabechi for their support and encouragement.

References

1. INTOR International Tokamak Reactor, Phase Two A, Part 1, 1983.
2. B.A. Cramer, et al., "An Approach for Determining the Lifetime of First Wall Structure in a Tokamak Reactor", Proc. of the Second Topical Meeting on the Technology of Controlled Nuclear Fusion", CONF-760935-P4, 1513(1976).
3. R.D. Watson, et al., "The Effect of Irradiation Creep, Swelling, Wall Erosion, and Embrittlement on the Fatigue Lifetime of a Tokamak First Wall", J. Nucl. Mater., 103, 97(1981).
4. R.F. Mattas, "Fusion Component Lifetime Analysis", Argonne National Laboratory Report ANL/FPP/TM-160(1982).
5. T. Horie, et al., "An Analytical and Experimental Study on Lifetime Predictions for Fusion Reactor First Walls and Divertor Plates", by T. Horie, et al., presented at the IAEA-TCM on Lifetime Predictions for the First Wall and Blanket Structure of Fusion Reactors, Karlsruhe, FRG, 5-7 November, 1985.
6. S. Majumdar, et al., "Thermal and Structural Limitations for Impurity Control Components in FED/INTOR", presented at the 7th International Conference on Structural Mechanics in Reactor Technology, Chicago, (1983).
7. Mizoguchi, T. and Itoh, S. "Bonded Protection Materials on the First Wall and Limiter/Divertor", presented at the IAEA Specialists, Meeting on Tokamak Concept Innovations, 13-17, Jan., 1986, Vienna.
8. Tolokan, R. et al., "Ceramic to Metal Attachment Using Low Modulus Brunsbond Pad", ASME Gas Turbine Division Meeting, Houston, Texas, March 9, 1981.
9. Private communication between J.R. Haines and T. Kobayashi (JAERI).
10. M.A. Abdou, et al., FED/INTOR Impurity Control and First Wall Engineering, FED-INTOR/ICFW/82-13(1982).
11. G.R. Hopkins, et al., "An Assessment of Carbon and Silicon Carbide as First Wall Materials in Inertial Confinement Fusion Reactors", GA-A14979, 1978.
12. Matsunami, N. et al., "Energy Dependence of the Ion-Induced Sputtering Yields of Monatomic Solids", Atomic Data and Nuclear Data Tables 31, 1-80, 1984.

13. J.N. Smith and C.H. Meyer, "Temperature Dependence of H_2^+ Sputtering of Coating on Pt", J. Nucl. Mater. 76 and 77, 193-8, 1978.

14. J. Roth, "Chemical Sputtering and Radiation Enhanced Sublimation of Graphite", Presented at the NATO Advanced Study Institute, International Course on the Physics of Plasma-Wall Interactions in Controlled Fusion, Quebec, August 1984.

Table 1 FIRST WALL AND DIVERTOR STUDY: ANALYSIS CASES

	CASE 1 FW Lo Dis. HEAT FLUX	CASE 2 FW HI Dis. HEAT FLUX	CASE 3 DIVERTOR BURN PHASE HI ROD. LOSS	CASE 3' DIVERTOR RECHARGE LOW EDGE TEMP	CASE 4 DIVERTOR BURN PHASE LOW RAD. TEMP	DASE 5 DIVERTOR RECHARGE HI EDGE TEMP	CASE 6 LIMITER
NORMAL OPERATION							
Peak heat flux (MW/m^2)	0.05-0.25-0.5	—	1.0-1.5-2.0	0.6-1.0	2.0-2.3-5.0	0.6-2.0	2.0-5.0
Peak ion flux $(m^{-2}-s^{-1})\times10^{23}$	0.02-0.18-0.35	—	0.1-0.47-2.5	0.1-0.6-2.5	0.5-1.9-15	0.002-0.014-0.3	0.05-1.5
Edge Temperature (eV)	60-200 (Neutral, Particle Energy)	—	5-20-50	5-20-50	5-20-50	50-300	50-300
Charge state of returing sputtered material	< 5	< 5	< 5	< 5	< 5	FULLY IONIZED	< 5
Fluence ($MW-yr/m^2$)	0.03-0.3	—	—	—	—	—	—
Burn time per pulse (s)	30-2000	—	30-2000	50-250-300	30-2000	50-250-300	30-2000
Number of cycles	10^3-10^4-10^5	—	—	—	—	—	—
DISRUPTION							
Peak energy density (MJ/m^2)	0.6-1.2	1.2-5.0	1.5-2.4-3.0	—	1.5-2.4-3.0	—	3.3
Duration (ms)	15-50	—	3-5		3-5		5
Number of disruptions	250-300-1000	—	250-300-1000	—	250-300-1000	—	250-1000

XXX-Indicates Nominal Value for FER

Table 2 DIVERTOR OPERATING CONDITIONS

	BURN PHASE	RECHARGE PHASE	
OPTION 1	CASE 3 HI RADIATION LOSS	CASE 3' LOW EDGE TEMPERATURE	← REFERENCE CONDITIONS FOR FER FY85
OPTION 2	CASE 3 HI RADIATION LOSS	CASE 5 HI EDGE TEMPERATURE	
OPTION 3	CASE 4 LOW RADIATION LOSS	CASE 3' LOW EDGE TEMPERATURE	
OPTION 4	CASE 4 LOW RADIATION LOSS	CASE 5 HI EDGE TEMPERATURE	

Table 3 Divertor Plate Conditions

Parameter	Range of Values
Normal Operation	
Peak Heat Flux (MW/m^2)	1.0 to 5.0 (1.5 Nominal)
Peak Ion Flux (m^{-2}-s^{-1})	5×10^{22} ($\frac{20}{T_{EDGE}}$)
Edge Temperature (eV)	5 to 300 (20 Nominal)
Burn time per pulse (s)	30 to 2000 (2000 Nominal)
Number of cycles	10^3 to 10^5
Fluence ($MW \cdot yr/m^2$)	0.03 to 0.3
Disruptions	
Peak Energy Density (MJ/m^2)	1.5 to 3.0 (2.4 Nominal)
Duration (ms)	5
Number of Disruptions	100 to 1000

Table 4 First Wall Conditions

Parameter	Range of Values
Normal Operation	
Peak Heat Flux (MW/m^2)	0.05 to 0.05 (0.25 Nominal)
Peak Neutral Particle Flux (m^{-2}-s^{-1})	1.8×10^{22}
Energy of Neutral Particles (eV)	60 to 200
Burn time per pulse (s)	30 to 2000 (2000 Nominal)
Number of cycles	10^3 to 10^5
Fluence ($MW \cdot yr/m^2$)	0.03 to 0.3
Disruptions	
Peak Energy Density (MJ/m^2)	0.02 to 5.0
Duration (ms)	15 to 50
Number of Disruptions	100 to 1000

Table 5 KEY ANALYSIS ASSUMPTIONS

	FW	DIVERTOR
COOLANT FLOW CONDITIONS		
- BULK COOLANT TEMP (°C)	40	40
- HEAT TRANSFER COEFFICIENT (W/m^2-K)	1.0×10^4	2.5×10^4
NEUTRON WALL LOADING (MW/m^2)	0.88	0.88
ARMOR THICKNESS (mm)	10 to 50	2 to 20
HEAT SINK FRONT PLATE THICKNESS (mm)	4	4
RADIATION FROM PLASMA FACING SURFACE		
- VIEW FACTOR	0.5	0.5
- TEMP. OF SURROUNDINGS (°C)	300	300
SPECIES MIX OF PARTICLES LEAVING PLASMA (%)	Burn phase	Recharge phase
- D	46.5	45
- T	46.5	45
- He	5	0
- O	1	10
CHARGE STATE OF IMPURITY IONS	2	2
CHARGE STATE OF RETURING SPUTTERD MATERIAL	4	4

Table 6 COMPLIANT LAYER PROPERTIES

	HITACHI CONCEPT	BRUNSBOND PAD
DENSITY (kg/m^3)	6100.	3115.
SPECIFIC HEAT (J/kg-K)	690.	446.
THERMAL CONDUCTIVITY (W/m-K)	240.	5.5 (@ 500 K)
EXPANSION COEFFICIENT (10^{-6}/K)	9.5	16.
YOUNG'S MODULUS (GPa)	76*	7.9

* ESTIMATED

Table 7 Selected divertor plate material/design options

ARMOR MATERIAL	HEAT SINK MATERIAL	ATTACHMENT CONCEPT
Beryllium	Copper alloy C17510	Bonded
Beryllium	V-15Cr-5Ti	↓
Graphite	OFHC-Copper	↓
Graphite	V-15Cr-5Ti	↓
Mo-TZM	OFHC-Copper	↓
Mo-TZM	V-15Cr-5Ti	↓
Silicon Carbide	OFHC-Copper	↓
Tungsten	OHFC-Copper	↓
Tungsten	Copper alloy C17510	↓
Tungsten	V-15Cr-5Ti	↓
Beryllium	OFHC-Copper	Compliant Layer
Graphite	↓	↓
Mo-TZM	↓	↓
Silicon Carbide	↓	↓
Tungsten	↓	↓

Table 8 Divertor Plate Performance for Option 1 Nominal Conditions

	ARMOR	HEAT SINK	NORMAL OPERATION			DISRUPTION		
			FATIGUE LIFETIME		EROSION LIFETIME (CYCLES)*	FATIGUE LIFETIME		EROSION LIFETIME** (DISRUPTIONS)
			ARMOR	HEAT SINK		ARMOR	HEAT SINK	
BRAZED	Be	Be-Cu	1.3×10^{6}	$> 10^{7}$	143	(1)	6.0×10^{5}	3100/197
	Be	V	< 10	1100	143	(1)	380	1900/120
	C	Cu	6.2×10^{5}	$> 10^{7}$	421	(1)	$> 10^{7}$	9.6×10^{5}
	C	V	$> 10^{7}$	$> 10^{7}$	421	(1)	$> 10^{7}$	1.3×10^{5}
	TZM	Cu	3.3×10^{4}	1.4×10^{6}	1700	(1)	7.6×10^{4}	$> 10^{7}$
	TZM	V	4.7×10^{4}	$> 10^{7}$	1700	(1)	$> 10^{7}$	$> 10^{7}$
	SiC	Cu	——	$> 10^{7}$	335	(1)	$> 10^{7}$	950/360
	W	Cu	$> 10^{7}$	3.8×10^{4}	3800	18	1.5×10^{4}	$> 10^{7}$
	W	Be-Cu	$> 10^{7}$	2.2×10^{6}	3800	18	1.4×10^{6}	$> 10^{7}$
	W	V	$> 10^{7}$	$> 10^{7}$	3800	18	$> 10^{7}$	$> 10^{7}$
HITACHI COMPLIANT LAYER DESIGN CONCEPT	Be	Cu	2.6×10^{5}	3.0×10^{6}	143	(1)	640	2980/210
	C	Cu	2.1×10^{6}	$> 10^{7}$	421	(1)	$> 10^{7}$	8.9×10^{5}
	TZM	Cu	3.6×10^{4}	3.0×10^{6}	1700	(1)	2.6×10^{5}	$> 10^{7}$
	SiC	Cu	——	$> 10^{7}$	335	(1)	$> 10^{7}$	928/346
	W	Cu	$> 10^{7}$	1.2×10^{5}	3800	22	4800	$> 10^{7}$

(1) THERMAL SHOCK DAMAGE EXPECTED

* BASED ON SPUTTERING EROSION DURING 2000 SECOND BURN/250 SECOND RECHARGE WITH NO REDEPOSITION

** VAPORIZATION LOSS/MELT LAYER LOSS

Table 9 Divertor Plate Performance for Option 2 Nominal Conditions

	ARMOR	HEAT SINK	NORMAL OPERATION			DISRUPTION		
			FATIGUE LIFETIME		EROSION LIFETIME (CYCLES)*	FATIGUE LIFETIME		EROSION LIFETIME** (DISRUPTIONS)
			ARMOR	HEAT SINK		ARMOR	HEAT SINK	
BRAZED	Be	Be-Cu	1.3×10^{6}	$> 10^{7}$	168	(1)	6.0×10^{5}	3000/209
	Be	V	< 10	1100	168	(1)	380	1850/113
	C	Cu	6.2×10^{5}	$> 10^{7}$	477	(1)	$> 10^{7}$	9.7×10^{5}
	C	V	$> 10^{7}$	$> 10^{7}$	477	(1)	$> 10^{7}$	1.3×10^{5}
	TZM	Cu	1060	$> 10^{7}$	— 0 —	(1)	4×10^{4}	$> 10^{7}$
	TZM	V	1520	$> 10^{7}$	— 0 —	(1)	$> 10^{7}$	$> 10^{7}$
	SiC	Cu	——	$> 10^{7}$	— 0 —	(1)	$> 10^{7}$	937/350
	W	Cu	$> 10^{7}$	3.8×10^{4}	— 0 —	39	1.5×10^{4}	$> 10^{7}$
	W	Be-Cu	$> 10^{7}$	2.2×10^{6}	— 0 —	38	1.4×10^{6}	$> 10^{7}$
	W	V	$> 10^{7}$	$> 10^{7}$	— 0 —	44	$> 10^{7}$	$> 10^{7}$
HITACHI COMPLIANT LAYER DESIGN CONCEPT	Be	Cu	2.6×10^{5}	3.0×10^{6}	168	(1)	640	2950/197
	C	Cu	2.1×10^{6}	$> 10^{7}$	477	(1)	$> 10^{7}$	8.8×10^{5}
	TZM	Cu	1160	$> 10^{7}$	— 0 —	(1)	2.0×10^{5}	$> 10^{7}$
	SiC	Cu	——	$> 10^{7}$	— 0 —	(1)	$> 10^{7}$	928/348
	W	Cu	$> 10^{7}$	1.2×10^{5}	— 0 —	36	4800	$> 10^{7}$

(1) THERMAL SHOCK DAMAGE EXPECTED

* BASED ON SPUTTERING EROSION DURING 2000 SECOND BURN/250 SECOND RECHARGE WITH NO REDEPOSITION

** VAPORIZATION LOSS/MELT LAYER LOSS

Table 10 Divertor Plate Performance for Option 3 Nominal Conditions

	ARMOR	HEAT SINK	NORMAL OPERATION			DISRUPTION		
			FATIGUE LIFETIME		EROSION LIFETIME (CYCLES)*	FATIGUE LIFETIME		EROSION LIFETIME (DISRUPTIONS)
			ARMOR	HEAT SINK		ARMOR	HEAT SINK	
BRAZED	Be	Be-Cu	< 10	9.1×10^5	40	(1)	1.3×10^5	2300/168
	Be	V	< 10	135	40	(1)	120	1190/ 86
	C	Cu	2.1×10^4	$> 10^7$	119	(1)	$> 10^7$	4.5×10^5
	C	V	4.9×10^4	$> 10^7$	119	(1)	$> 10^7$	2.9×10^4
	TZM	Cu	1.0×10^4	4.1×10^4	711	(1)	3000	$> 10^7$
	TZM	V	1.5×10^4	9×10^6	711	(1)	3.6×10^6	$>10^7$/654
	SiC	Cu	——	$> 10^7$	98	(1)	$> 10^7$	786/317
	W	Cu	5.5×10^5	850	1740	23	340	$> 10^7$
	W	Be-Cu	4.0×10^5	3.4×10^5	1740	22	1.4×10^5	$> 10^7$
	W	V	5.4×10^5	3.0×10^6	1740	28	5.4×10^5	$> 10^7$
HITACHI COMPLIANT LAYER DESIGN CONCEPT	Be	Cu	< 10	2000	40	(1)	260	2210/172
	C	Cu	8.1×10^4	$> 10^7$	119	(1)	$> 10^7$	3.8×10^5
	TZM	Cu	1.1×10^4	1.2×10^5	711	(1)	6860	$> 10^7$
	SiC	Cu	——	$> 10^7$	98	(1)	2.2×10^6	768/290
	W	Cu	6.0×10^5	1600	1740	21	430	$> 10^7$

* BASED ON SPUTTERING EROSION DURING 2000 SECOND BURN/250 SECOND RECHARGE WITH NO REDEPOSITION

** VAPORIZATION LOSS/MELT LAYER LOSS

(1) THERMAL SHOCK DAMAGE EXPECTED

Table 11 Divertor Plate Performance for Option 4 Nominal Conditions

	ARMOR	HEAT SINK	NORMAL OPERATION			DISRUPTION		
			FATIGUE LIFETIME		EROSION LIFETIME (CYCLES)*	FATIGUE LIFETIME		EROSION LIFETIME (DISRUPTIONS)
			ARMOR	HEAT SINK		ARMOR	HEAT SINK	
BRAZED	Be	Be-Cu	< 10	9.1×10^{5}	42	(1)	1.3×10^{5}	2240/186
	Be	V	< 10	135	42	(1)	120	1200/86
	C	Cu	2.1×10^{4}	$> 10^{7}$	123	(1)	$> 10^{7}$	4.5×10^{5}
	C	V	4.9×10^{4}	$> 10^{7}$	123	(1)	$> 10^{7}$	2.9×10^{4}
	TZM	Cu	330	2.1×10^{4}	- 0 -	(1)	1700	$> 10^{7}$
	TZM	V	470	9×10^{6}	- 0 -	(1)	3.6×10^{6}	$>10^{7}$/664
	SiC	Cu	——	$>10^{7}$	- 0 -	(1)	$> 10^{7}$	$> 10^{7}$
	W	Cu	5.5×10^{5}	850	- 0 -	23	340	$> 10^{7}$
	W	Be-Cu	4.0×10^{5}	3.4×10^{5}	- 0 -	22	1.4×10^{5}	$> 10^{7}$
	W	V	5.4×10^{5}	3.0×10^{6}	- 0 -	28	5.4×10^{5}	$> 10^{7}$
HITACHI COMPLIANT LAYER DESIGN CONCEPT	Be	Cu	<10	2000	42	(1)	260	2210/172
	C	Cu	8.1×10^{4}	$> 10^{7}$	123	(1)	$> 10^{7}$	3.8×10^{5}
	TZM	Cu	360	6.6×10^{4}	- 0 -	(1)	3400	$> 10^{7}$
	SiC	Cu	——	$> 10^{7}$	- 0 -	(1)	2.2×10^{6}	768/290
	W	Cu	6.0×10^{5}	1600	- 0 -	21	430	$> 10^{7}$

* BASED ON SPUTTERING EROSION DURING 2000 SECOND BURN/250 SECOND RECHARGE WITH NO REDEPOSITION

** VAPORIZATION LOSS/MELT LAYER LOSS

Table 12 Qualitative Comparison of first wall design concepts

Concept	Major Advantage	Major Limitation
Bare metal wall	- Simplicity	- Damage of primary coolant structure during disruptions
Radiation cooled armor	- Simple design if armor required - Remote maintenance in-situ is possible	- Temperature limits heat flux that can be tolerated
Armor Bonded to Cooled structure	- Low temperature operation	- Difficult fabrication - Difficult maintenance
Armor bonded to cooled structure with intermediate compliant layer	- Low temperature operation - Low thermal stresses during fabrication and operation	- Complex Fabrication - Difficult maintenance

Table 13 Recommended divertor plate design concepts

Plasma Edge Temperature Range (eV)	Heat Flux Range (MW/m^2)	Recommended Materials Armor/Heat Sink
< 40	< 1.5	Tungsten/OFHC-Copper
< 40	1.5 to 5.0	Tungsten/Copper alloy C17510
< 50	1.5 to 5.0	Mo-TZM/V-15Cr-5Ti
> 50	$\lesssim 2.0$	Graphite/OFHC-Cooper
> 50	$\gtrsim 2.0$	Graphite/OFHC-Copper with a Compliant layer (Performance is questionable at fluence $\gtrsim 0.03$ MW·yr/m^2)

Table 14 SUMMARY OF RECOMMENDED DIVERTOR PLATE MATERIALS

OPTION	BURN/RECHARGE CONDITIONS	ARMOR/HEAT SINK
1	HI RAD/LOW TEMP DIVERTOR	W/Cu (TZM/V IF T_{EDGE} > 40 eV)
2	HI RAD/HI TEMP DIVERTOR	W/Cu
3	LOW RAD/LOW TEMP DIVERTOR	W/Be-Cu (C/Cu IF T_{EDGE} > 40 eV) (WITH COMPLIANT LAYER)
4	LOW RAD/HI TEMP DIVERTOR	C/Cu (WITH COMPLIANT LAYER)
Case 6	Pumped Limiter	C/Cu (WITH COMPLIANT LAYER)

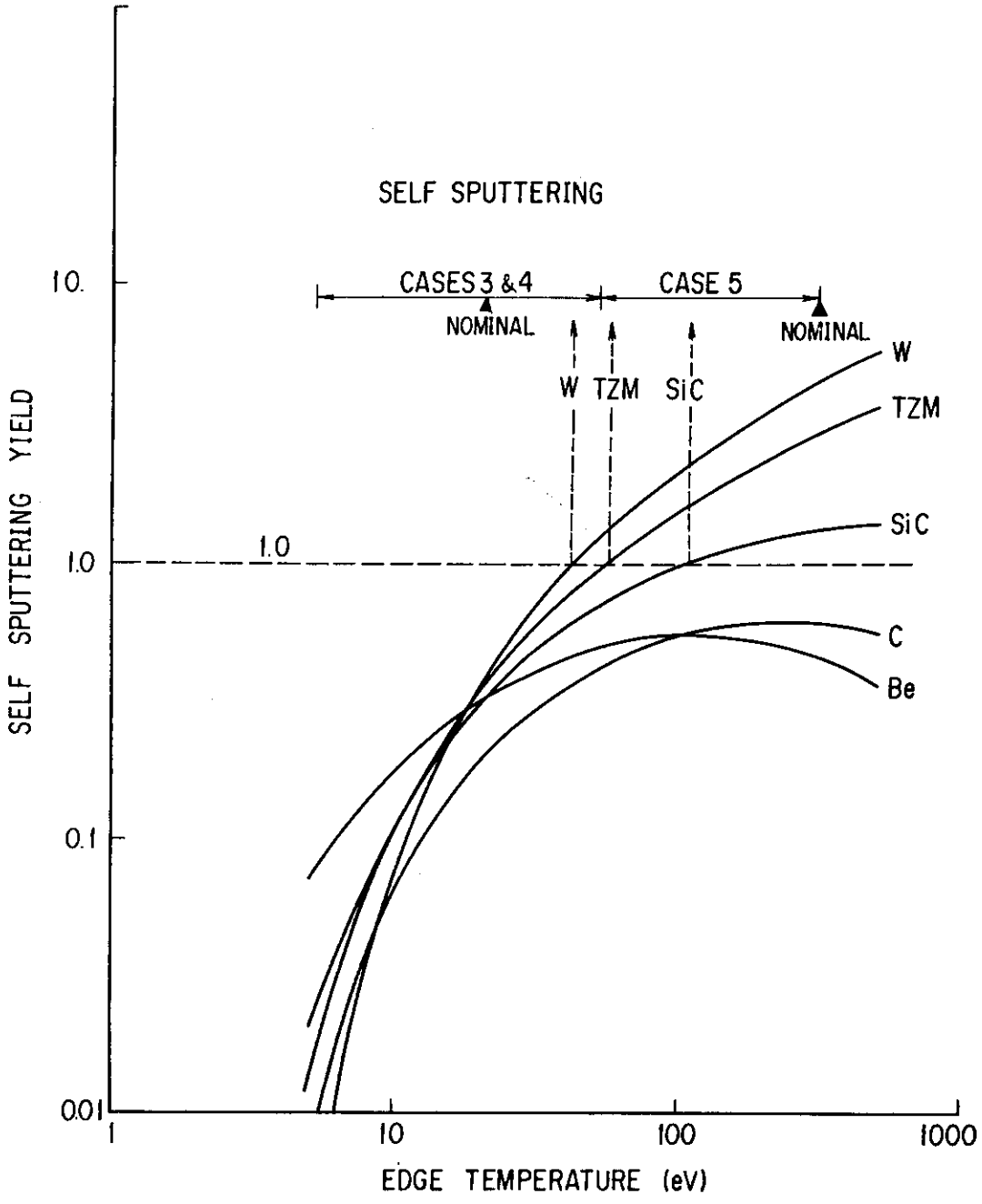

Fig. 1 Self sputtering yields for candidate armor materials

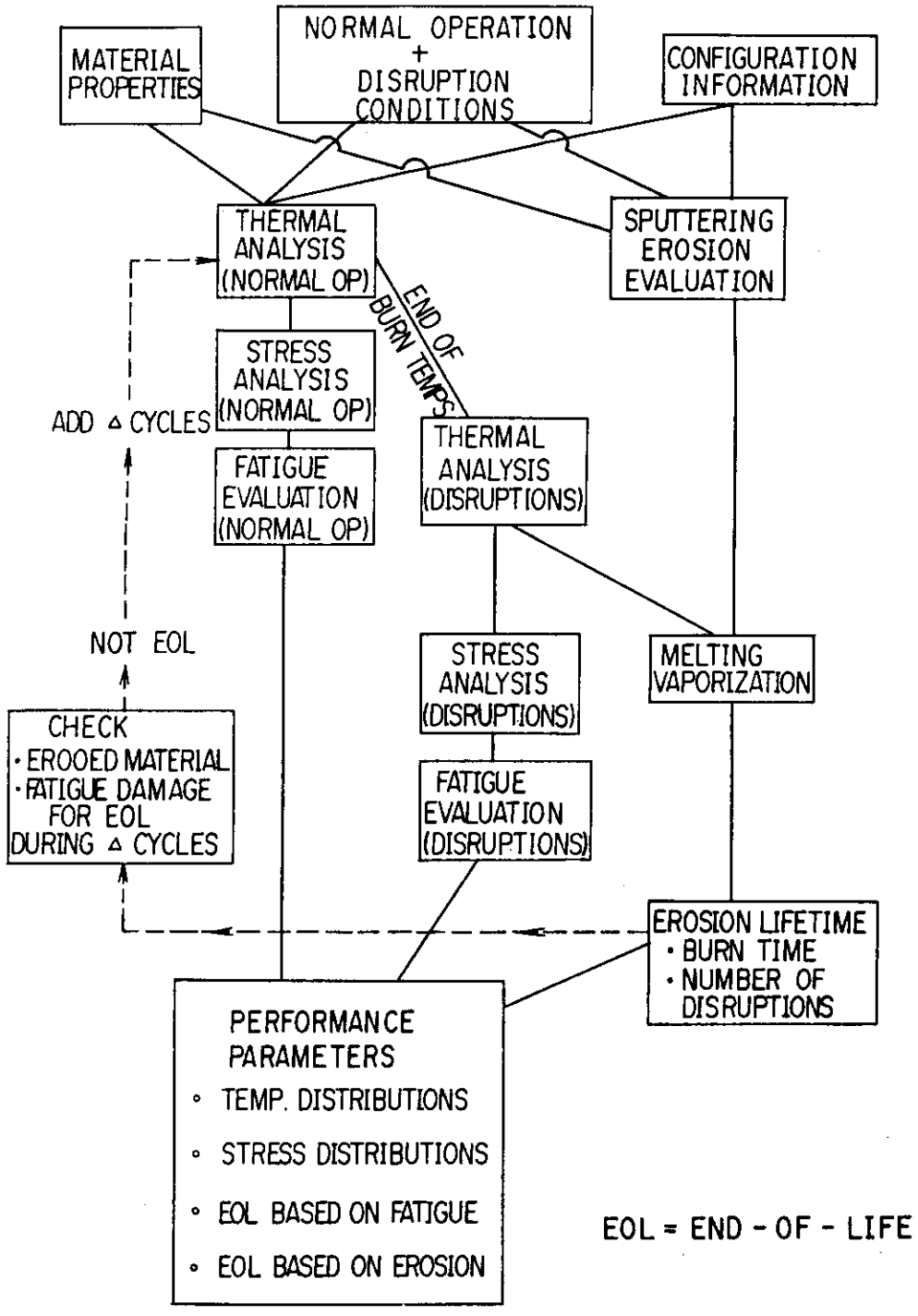

Fig. 2 Computer code flow diagram

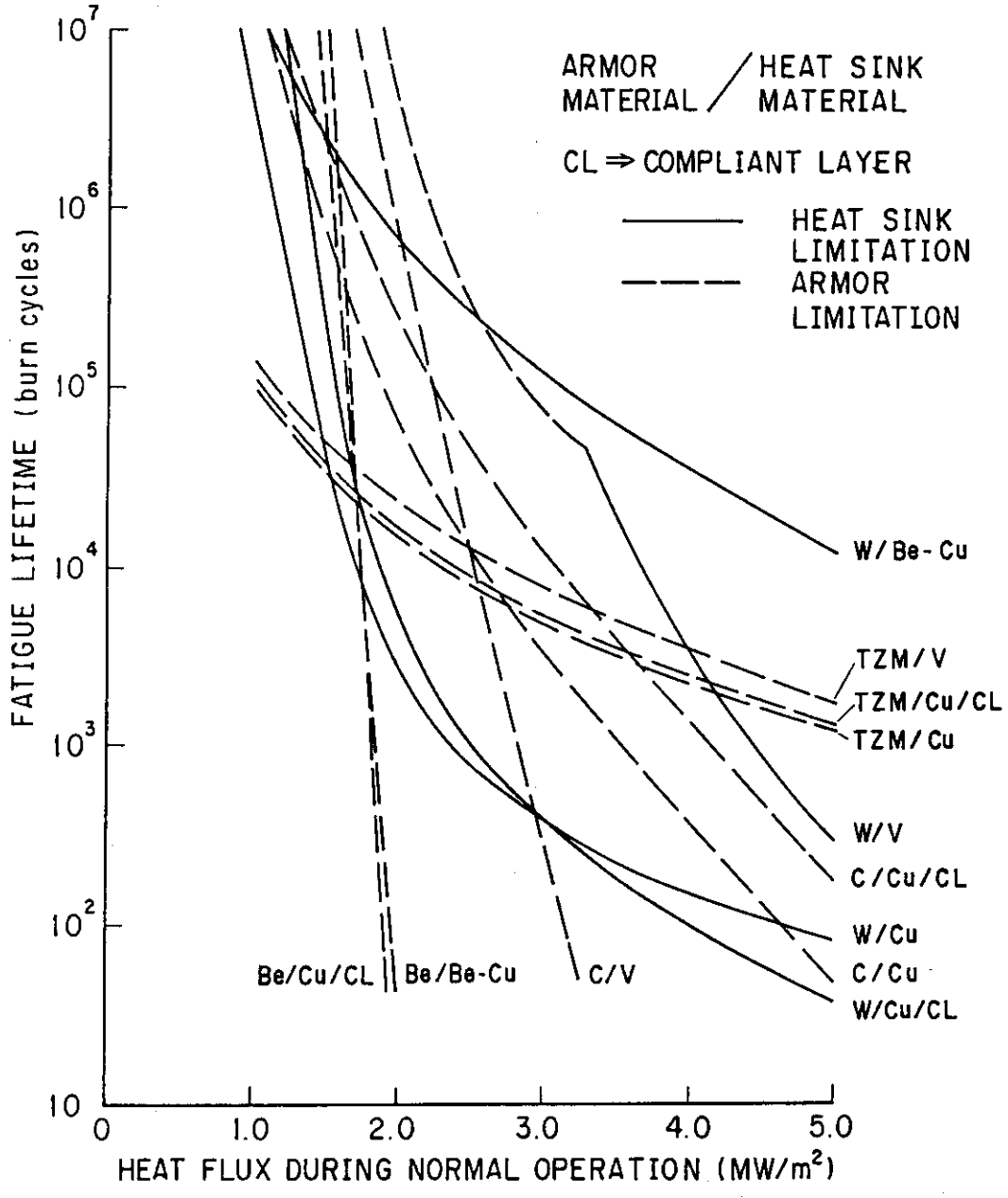

Fig. 3 Fatigue lifetime performance of divertor plate candidate materials

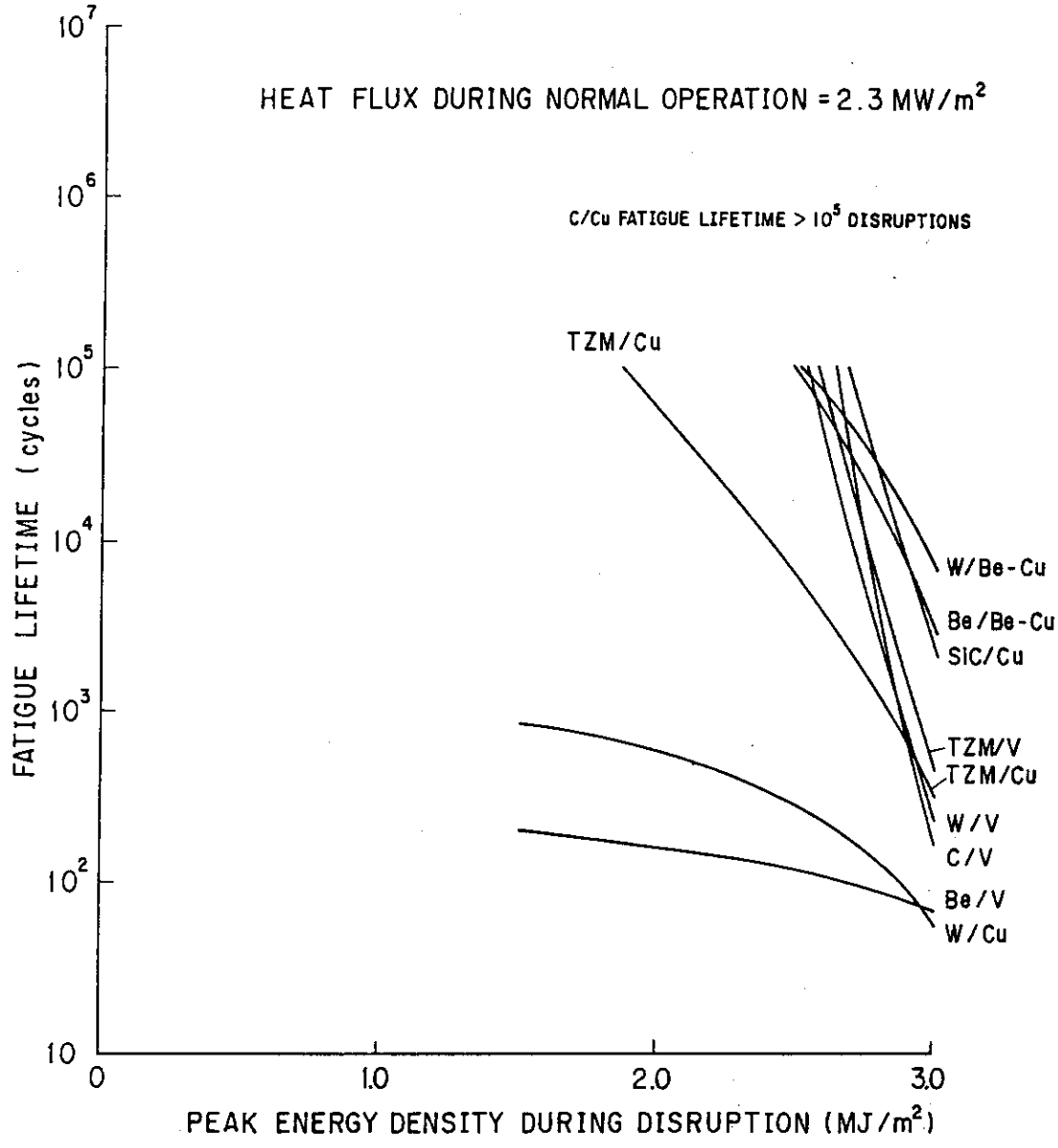

Fig. 4 Disruption fatigue lifetime of divertor plate material candidates

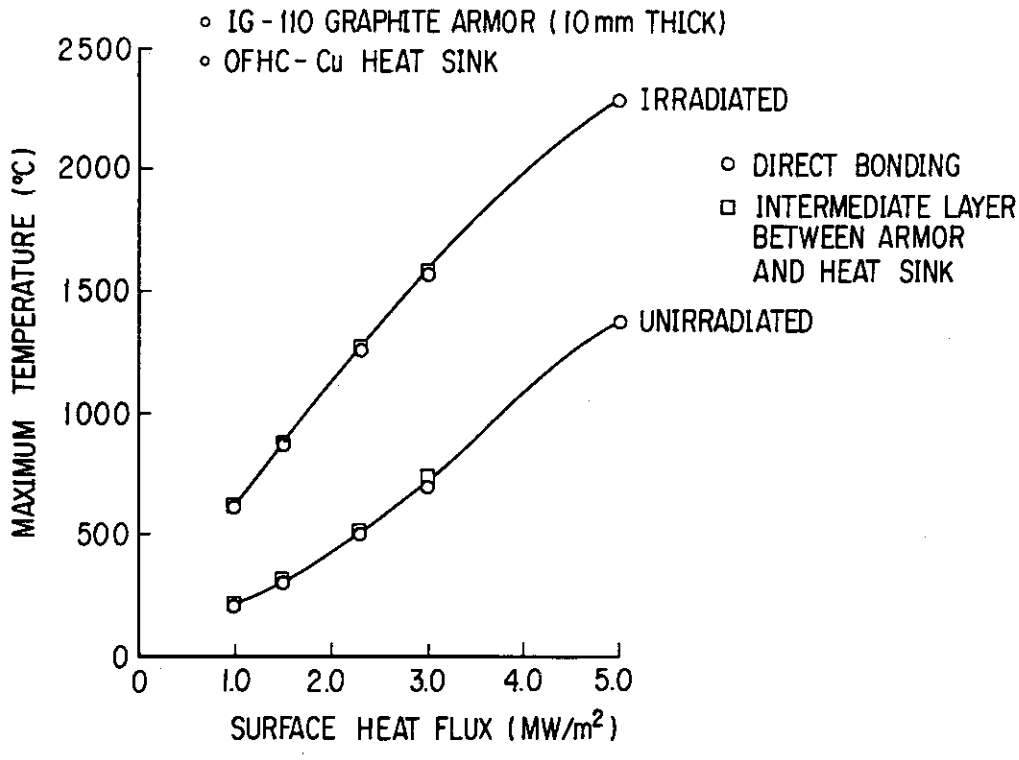

Fig. 5 Effect of radiation damage on graphite armor temperatures

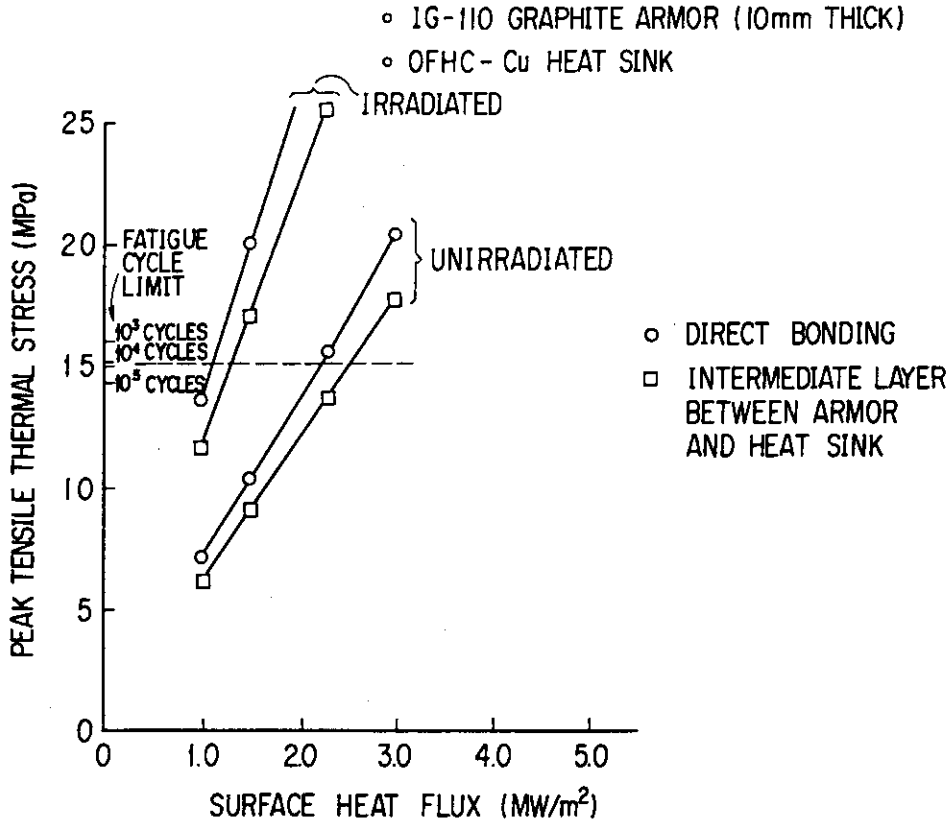

Fig. 6 Effect of radiation damage on graphite armor thermal stresses

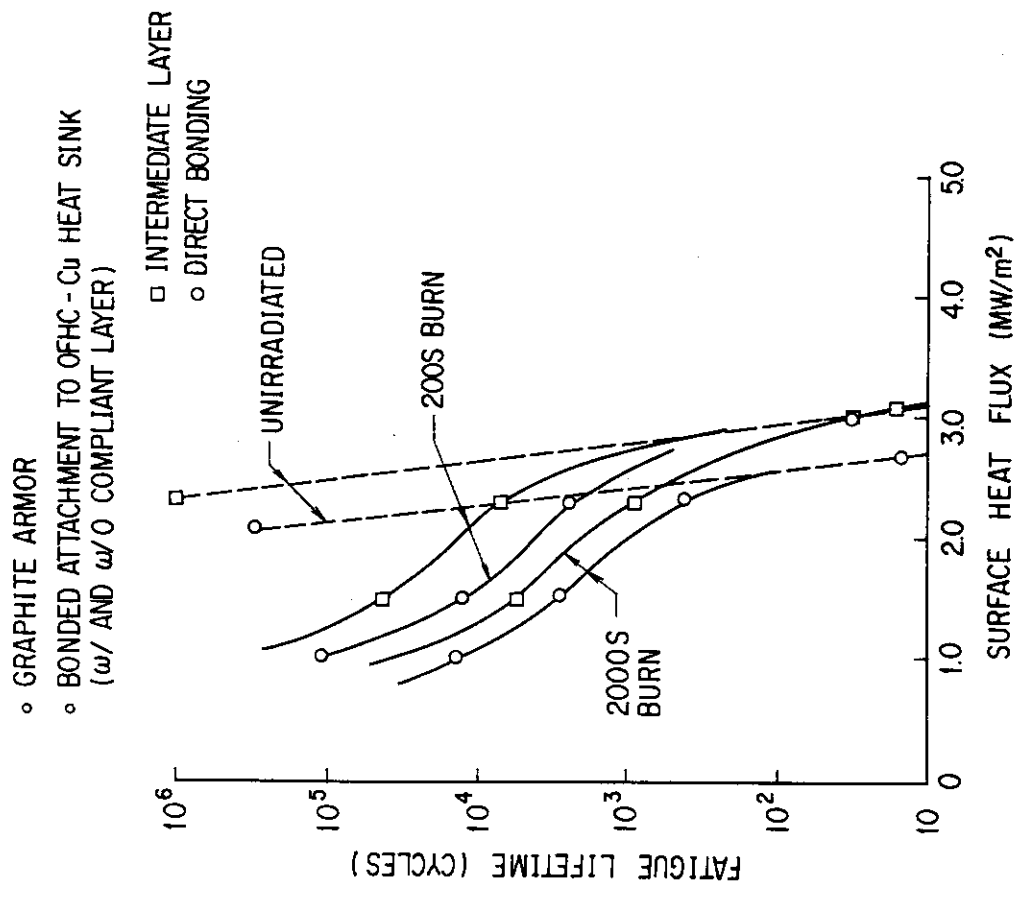

Fig. 7 Fatigue/Radiation damage performance for graphite (IG-110)

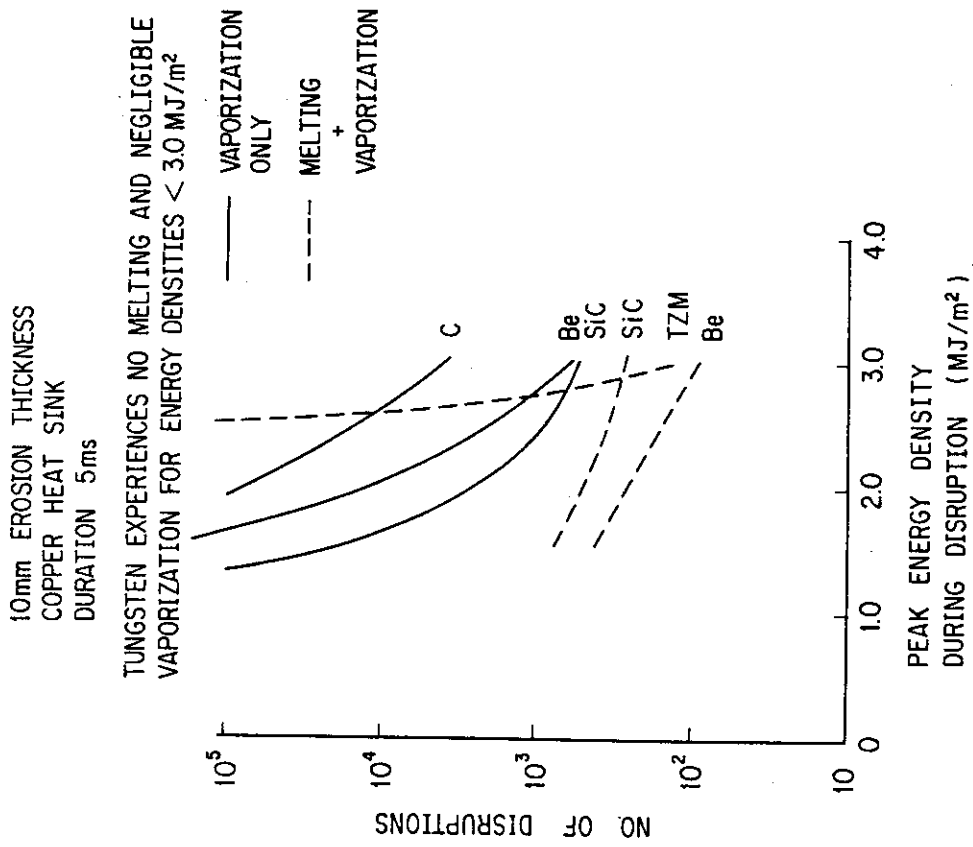

Fig. 8 Disruption induced erosion of divertor plate materials

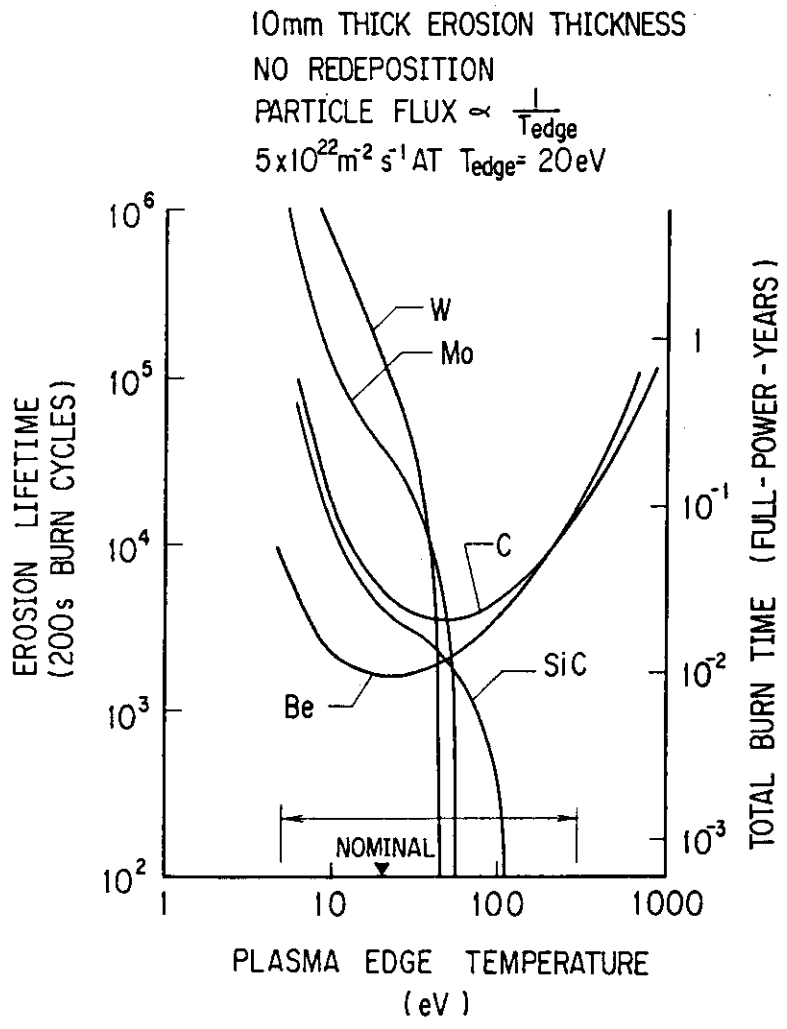

Fig. 9 Sputtering erosion lifetimes for divertor plate

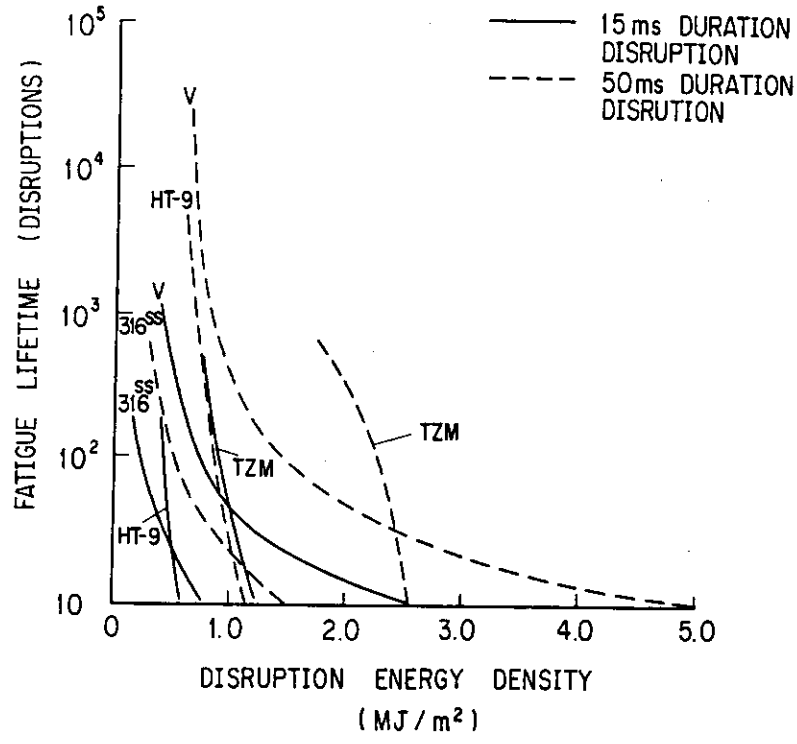

Fig. 10_a Fatigue lifetime of bare metal first walls during plasma disruptions

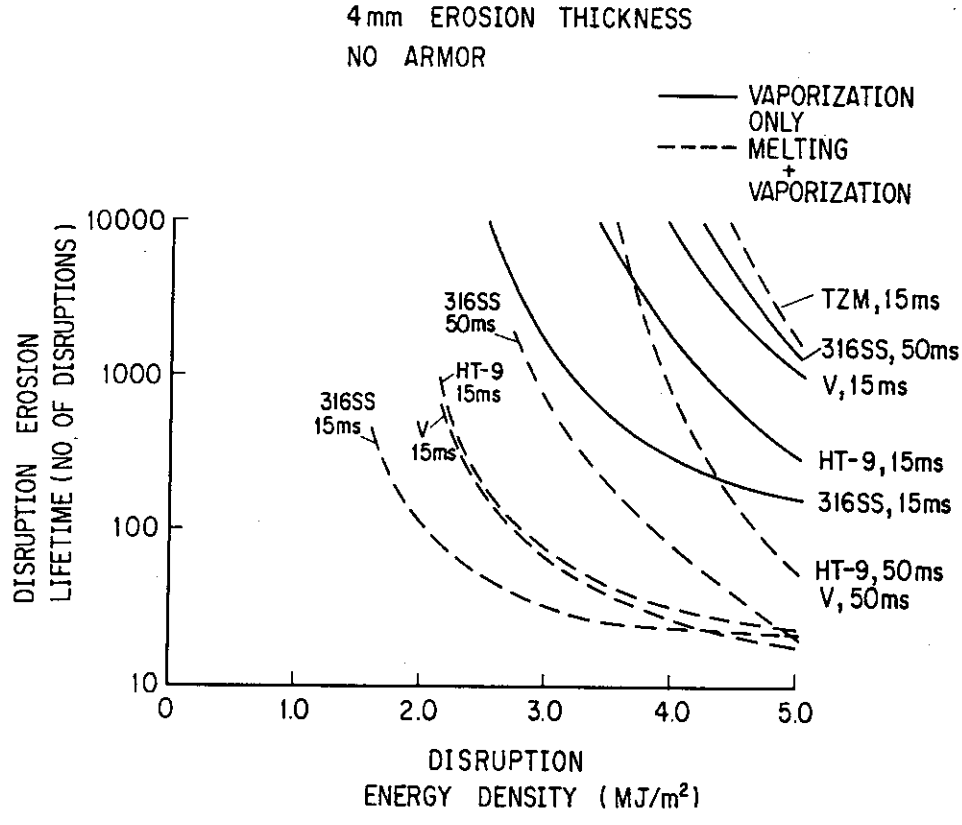

Fig. 10_b Disruption induced erosion lifetimes of bare metal first wall candidates

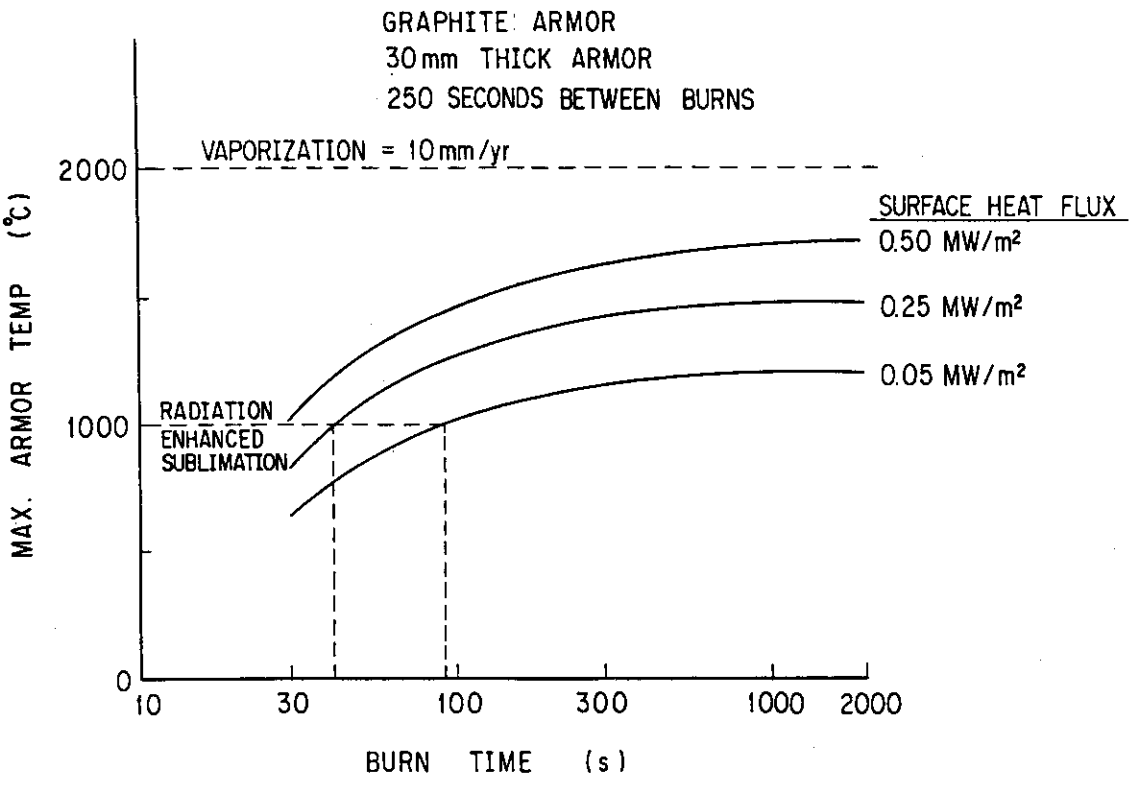

Fig. 11 Thermal performance of radiation cooled graphite (GRAPHNOL-N3M) inboard first wall armor

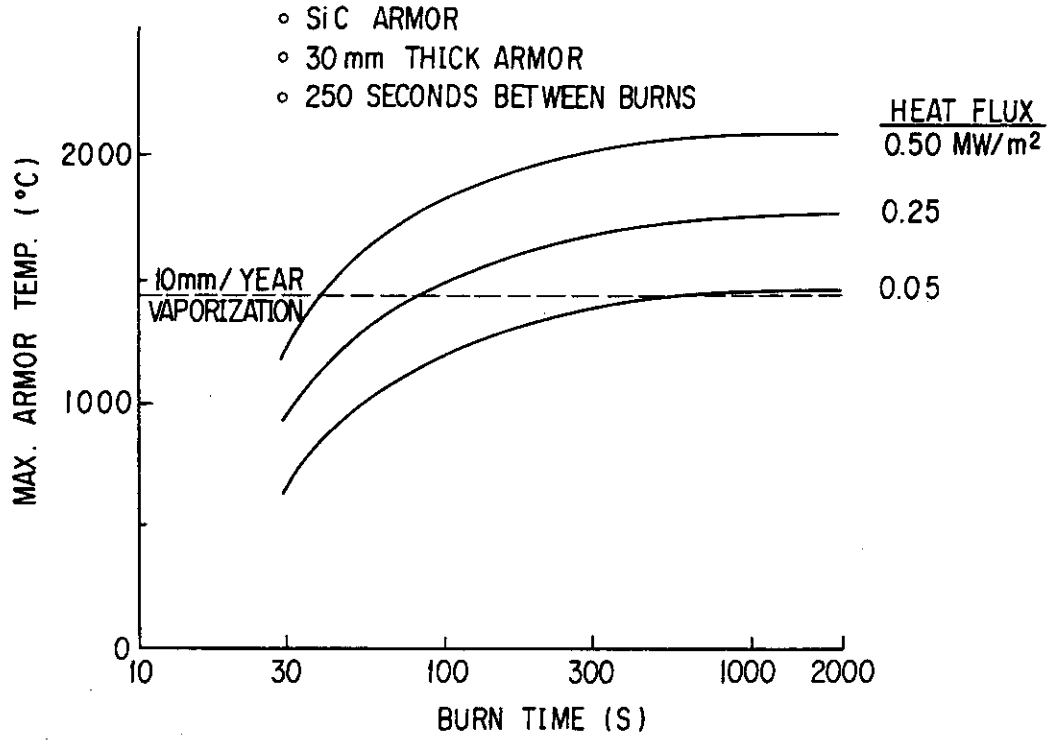

Fig. 12 Thermal performance of radiation cooled SiC inboard first wall armor

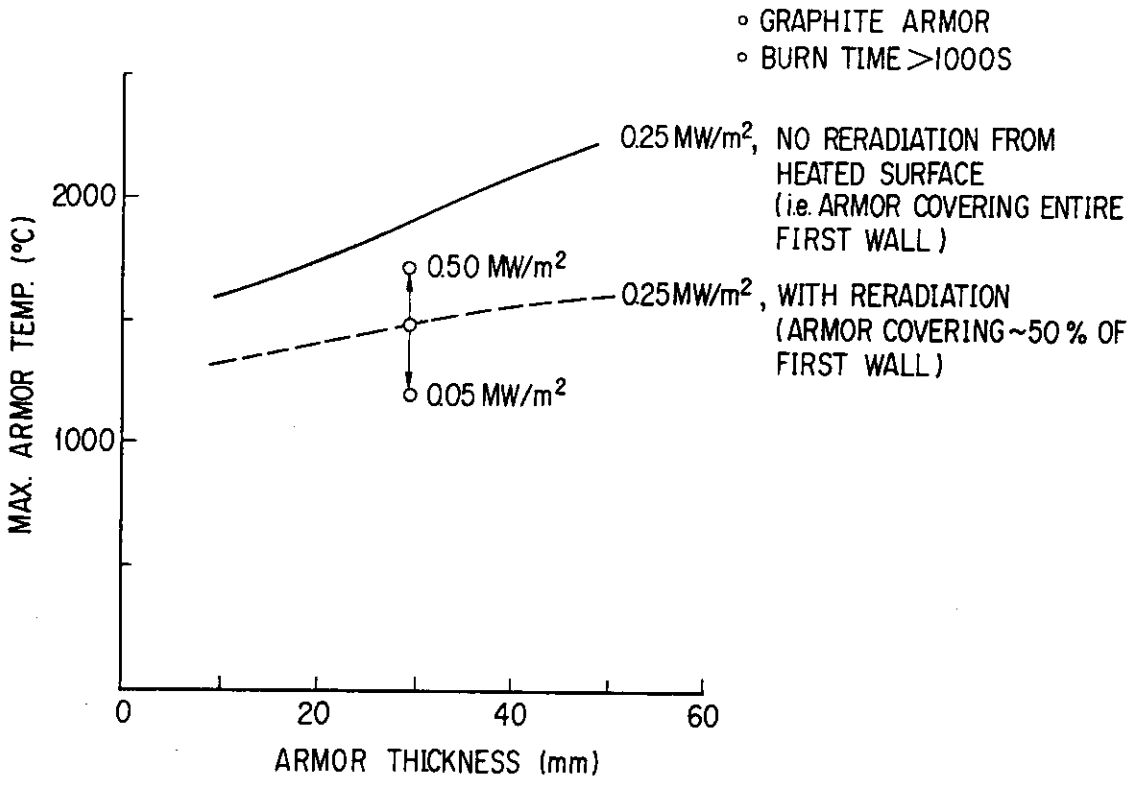

Fig. 13 Thermal performance of radiation cooled graphite armor covering the entire first wall

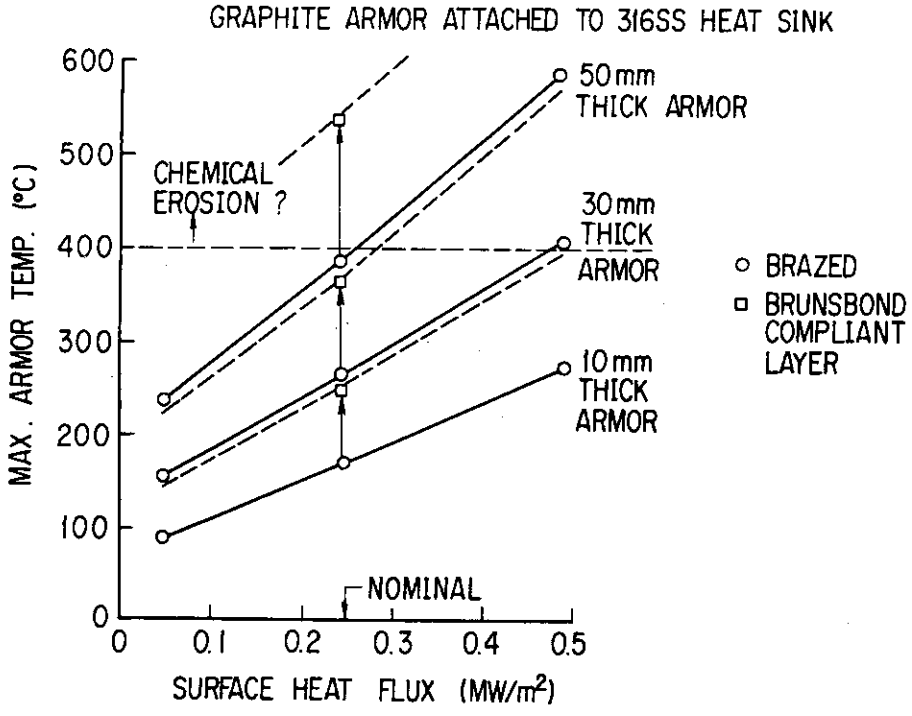

Fig. 14 Graphite armor (Unirradited GRAPHNOL-N3M) surface temperature for bonded attachment concepts

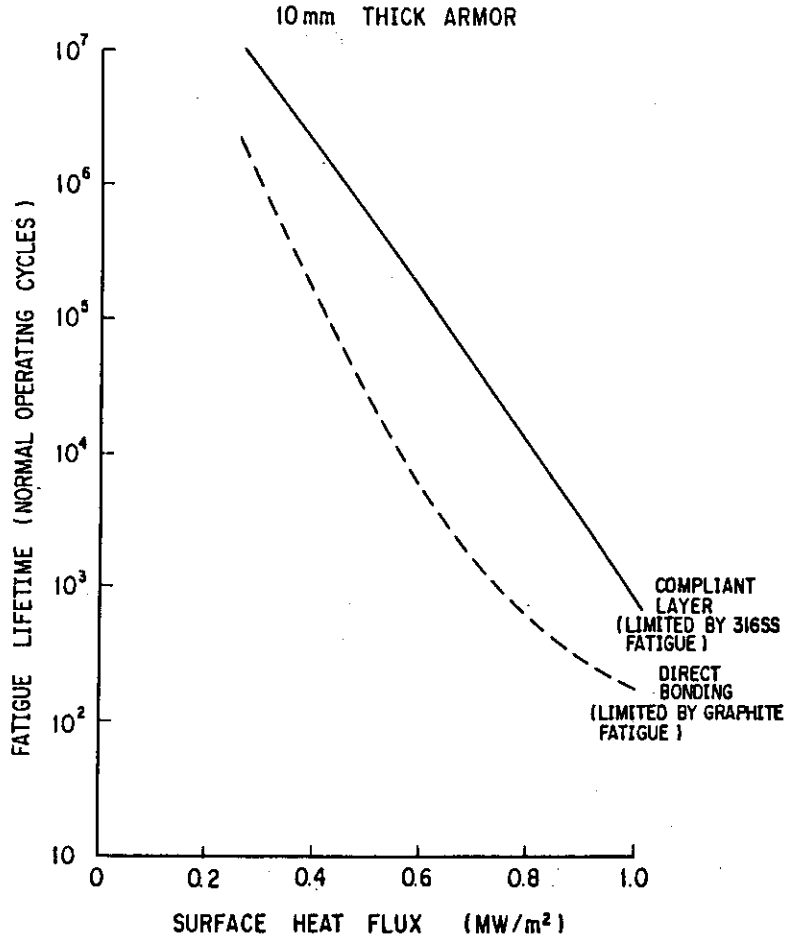

Fig. 15 Fatigue lifetime of graphite (unirradiated GRAPHNOL-N3M) bonded to 316SS as a function of first wall heat flux

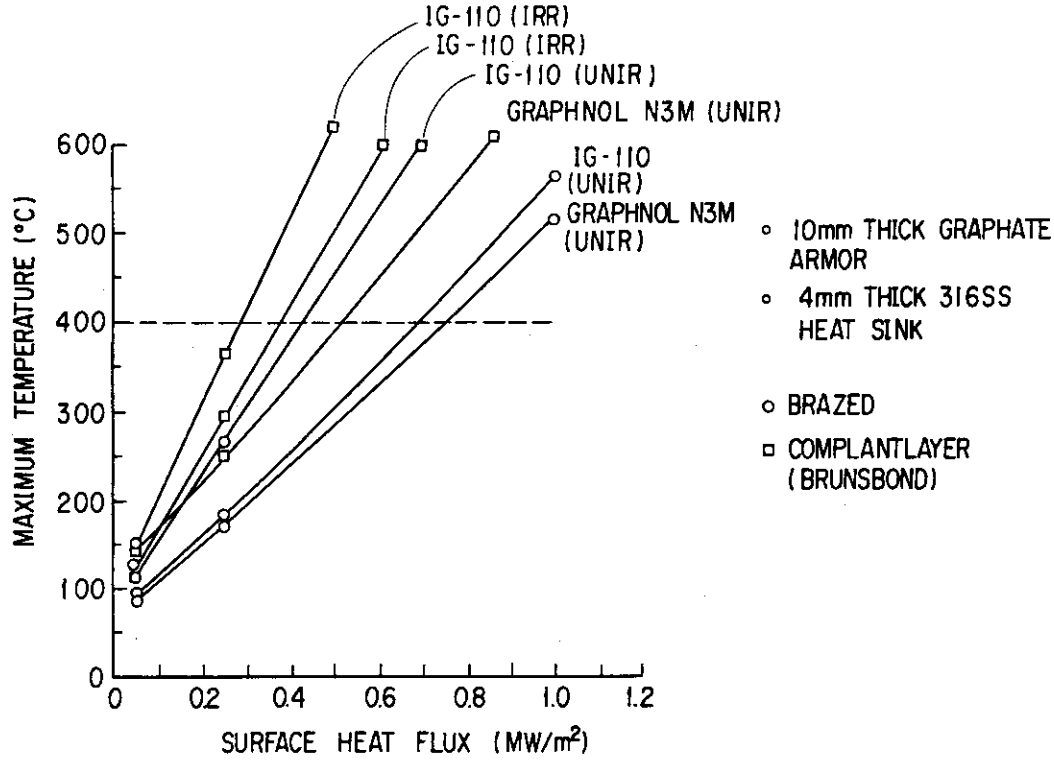

Fig. 16 Effect of radiation damage on graphite first wall armor temperatures

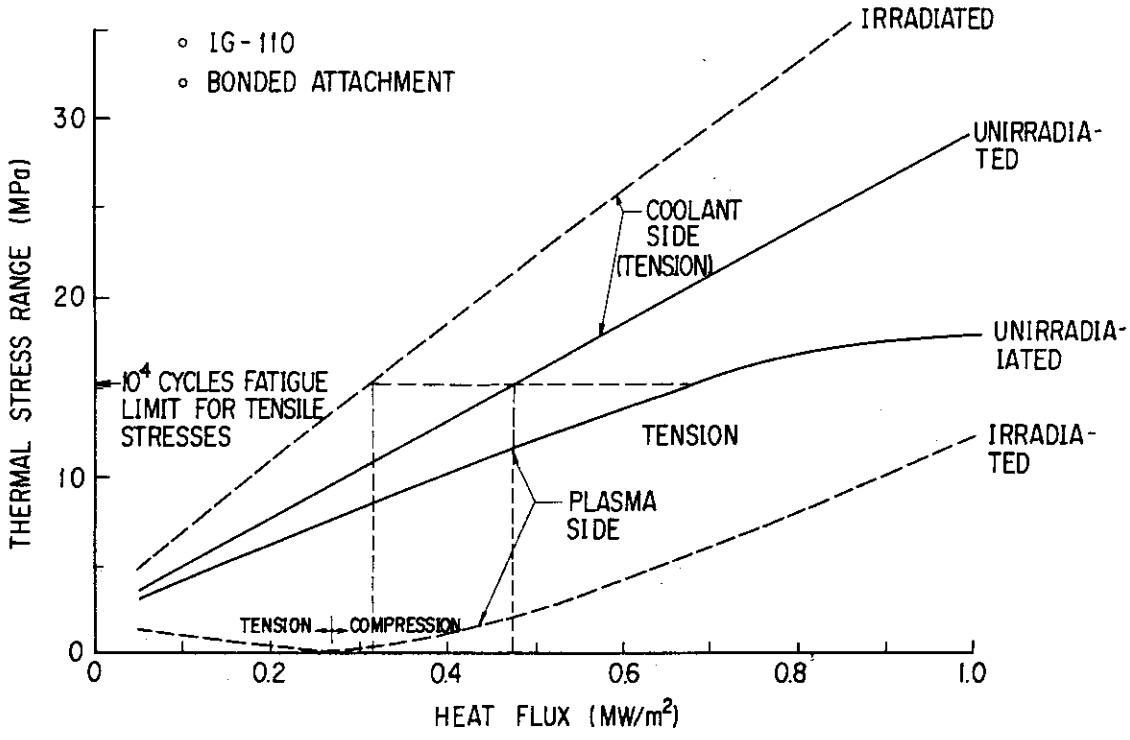

Fig. 17 Effect of radiation damage on thermal stresses in graphite armor (direct bonding design concept)

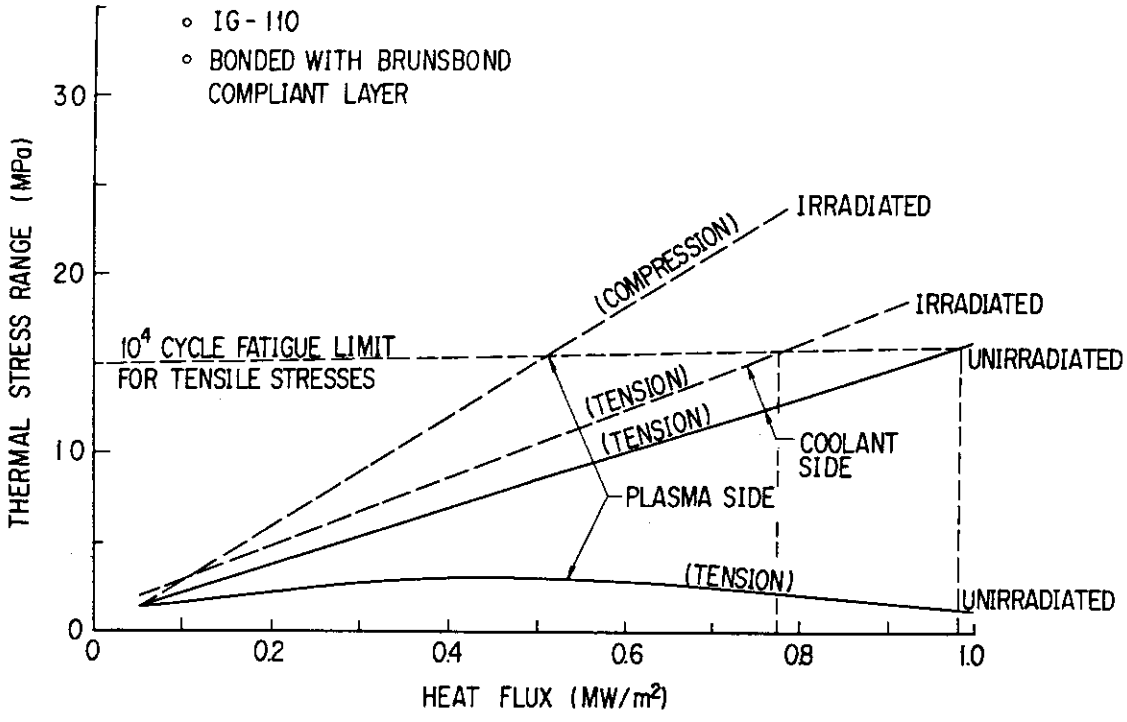

Fig. 18 Effect of radiation damage on graphite armor thermal stresses (compliant layer concept)

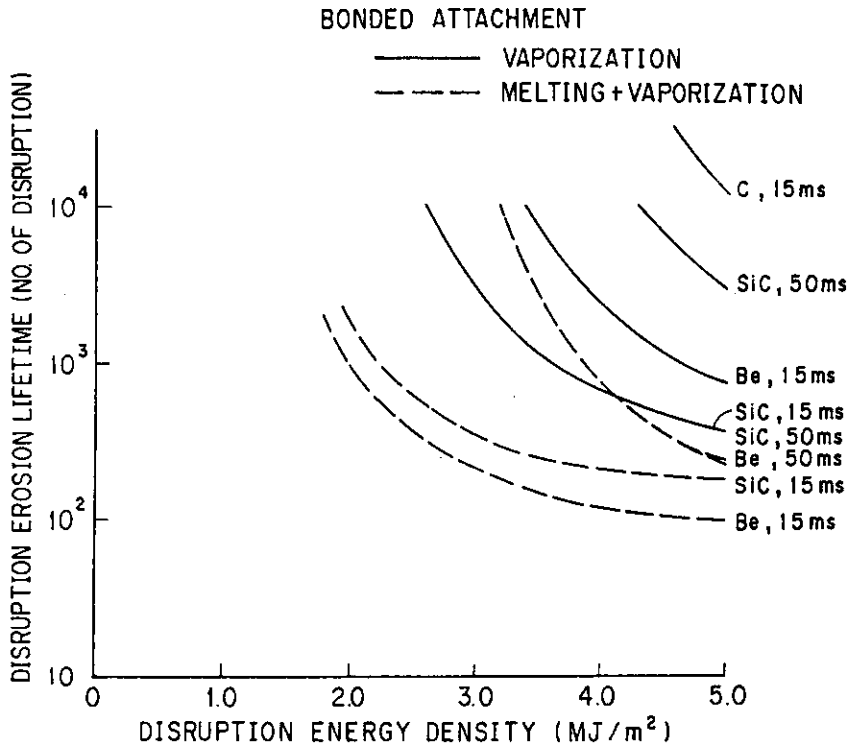

Fig. 19 Disruption induced erosion lifetimes of candidate first wall armor materials

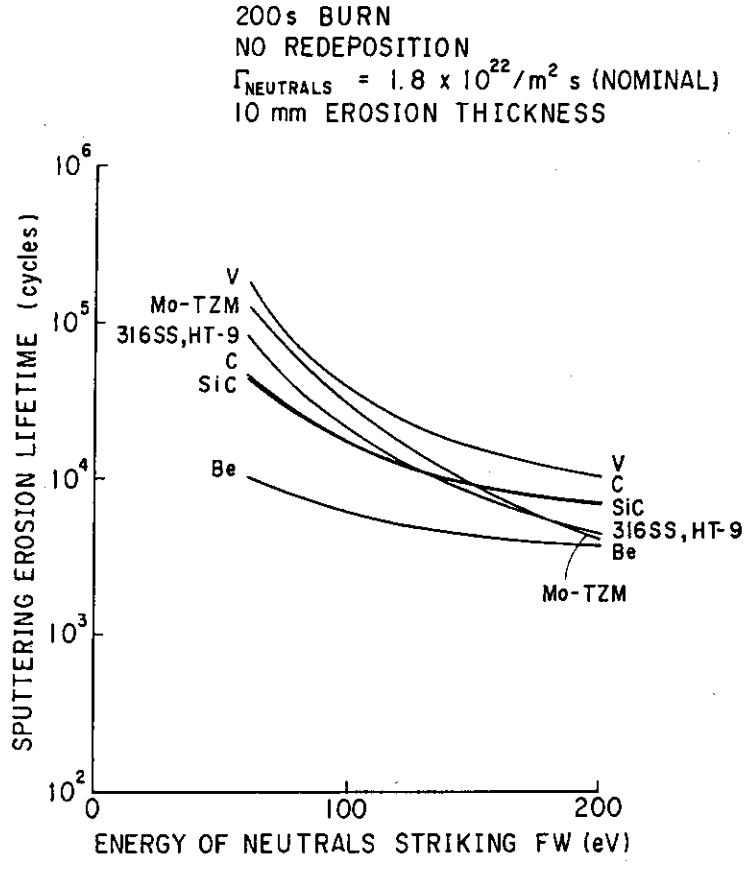

Fig. 20 Sputtering erosion lifetimes of candidate first wall armor materials

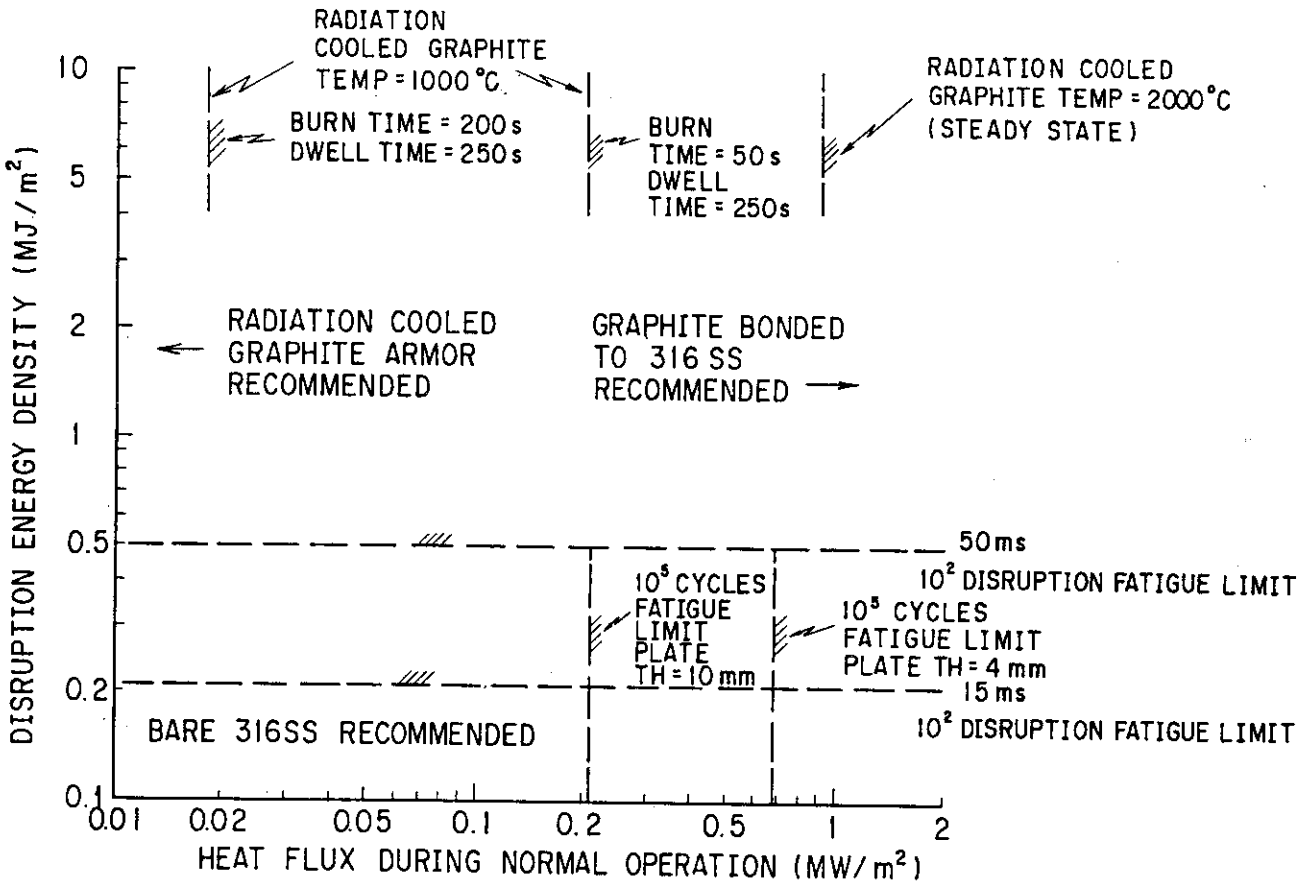

Fig. 21 Recommended first wall materials and design features (316 SS structure)

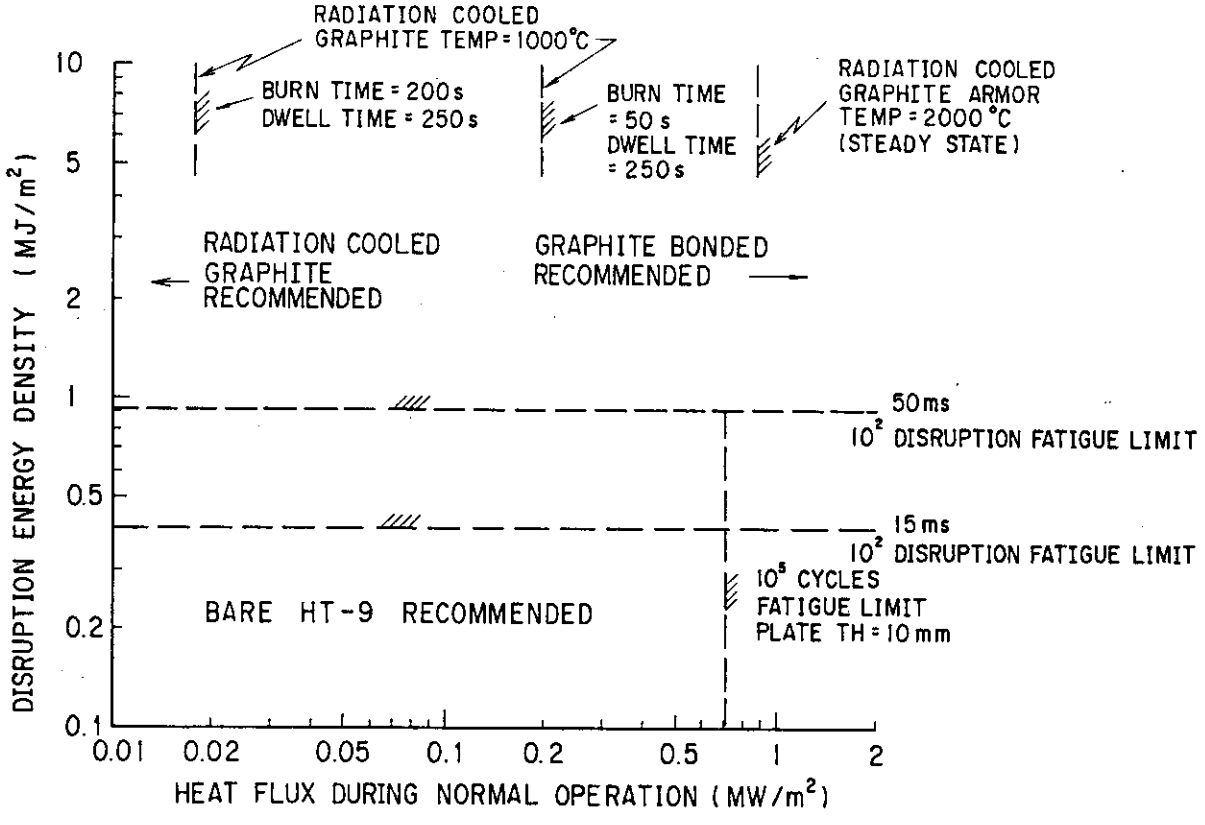

Fig. 22 Recommended first wall materials and design features (HT-9 structure)

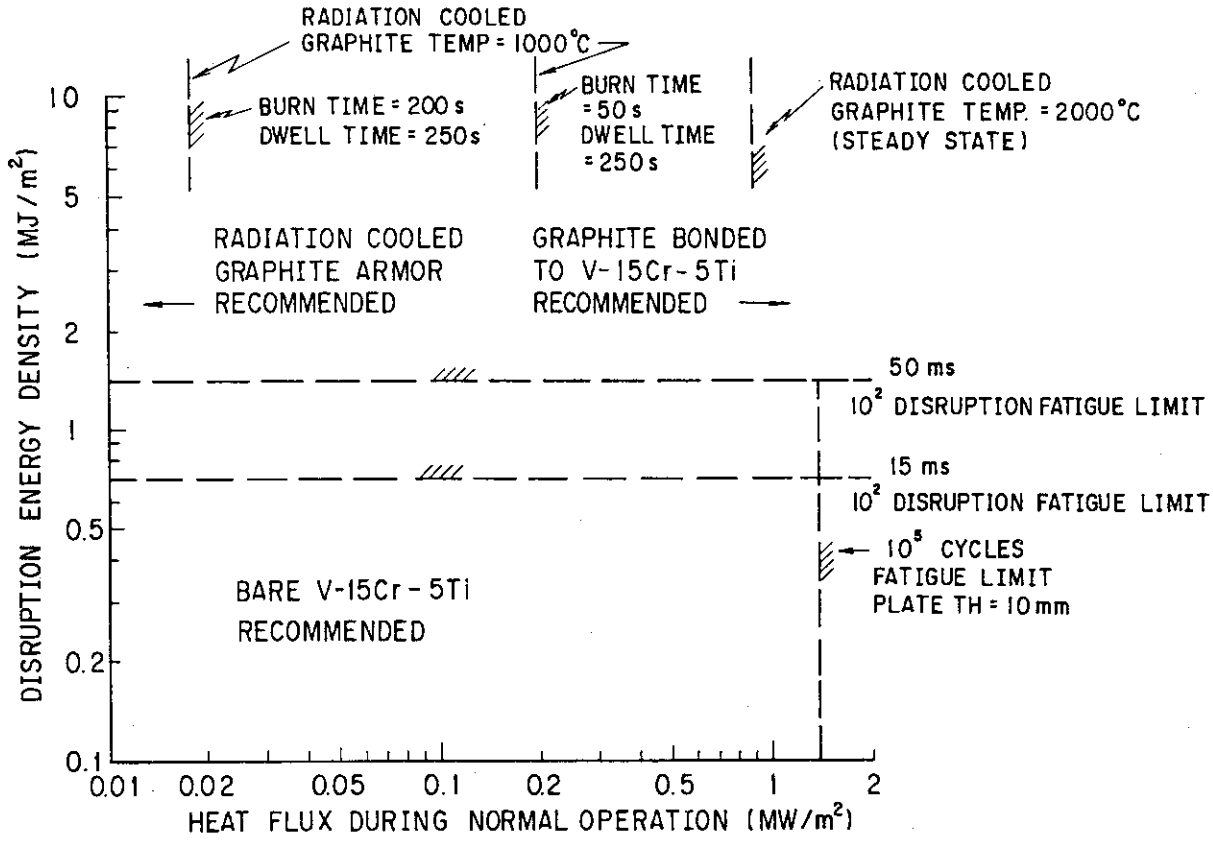

Fig. 23 Recommended first wall materials and design features (V-15Cr-5Ti structure)

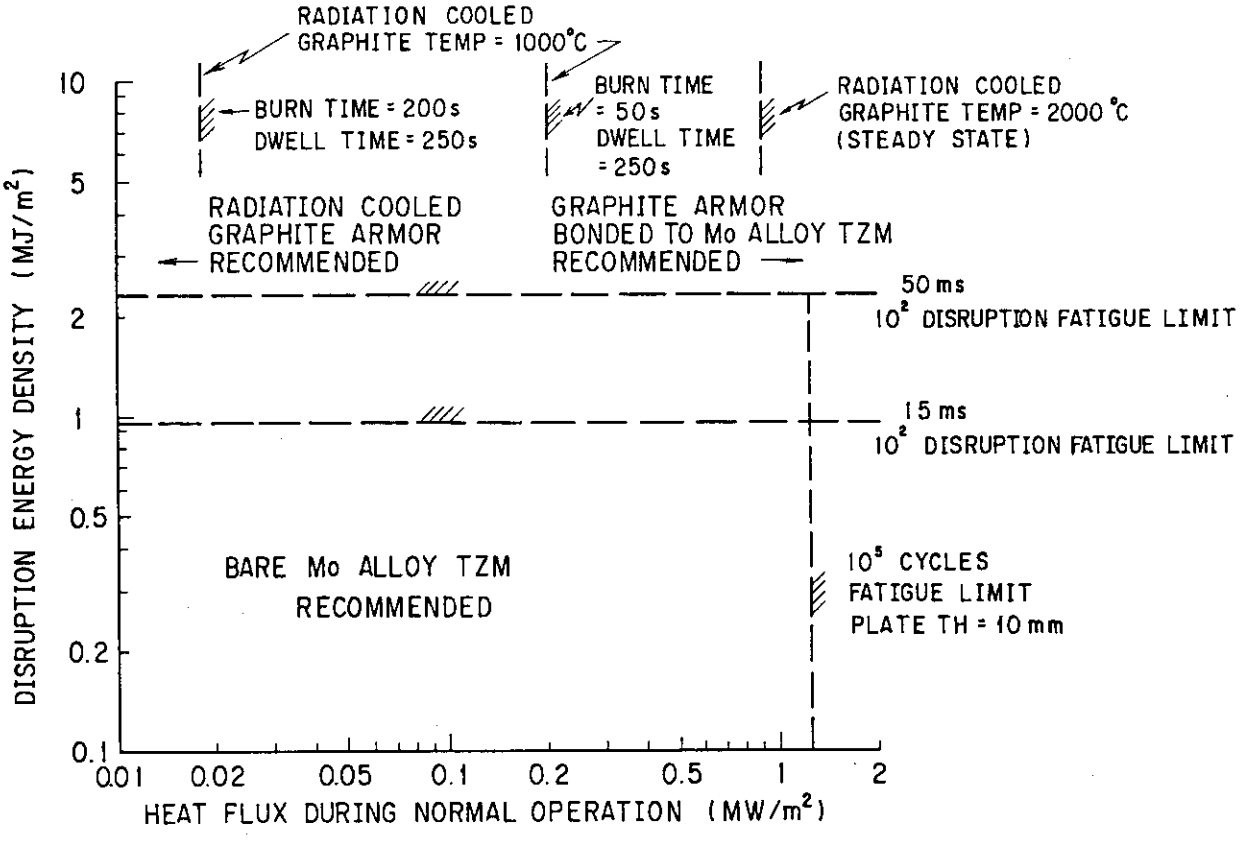

Fig. 24 Recommended first wall materials and design features (Mo alloy TZM structure)

Appendix A. Material Properties

Properties for all materials considered in this study are listed in Tables A-1 and A-2. In general, temperature dependence of properties such as, specific heat, thermal conductivity, expansion coefficient, and elastic modulus, was included. References are indicated at the bottom of Table A-2 for each material. As indicated in these tables, some properties were not available and were therefore estimated. The relatively large number of estimated properties points to the need for improvement in the data base.

Properties for IG-110 graphite[A-16] in the urirradiated conditoin, as well as the properties after irradiation to a fluence of 3.0×10^{25} n/m^2 are presented in Tables A-1 and A-2. Since strain limited fatigue data were not available, the stress limited fatigue data for IG-110, presented in Figure A-1, were used in this study. Fatigue data for IG-110 are a very strong function of R, which is the ratio of minimum stress to maximum stress. At the interface between the armor and heat sink materials R is generally equal to zero, i.e. stresses are tensile during the entire burn cycle and also during disruptions. At the heated surface, the value of R during normal operation varies from o to $-\infty$, depending upon the armor thickness, heating conditions, and heat sink material. However, during disruptions the heated surface experiences a very large compressive stress. Thus, R approaches $-\infty$ during the disruption cycle.

A-1. Metals Handbook, 8th Edition, Vol. 1, Properties and Selection of Metals, American Society for Metals, 1961.

A-2. Selected Values of Thermodynamic Properties of Metals and Alloys, by R. Hultgren et al., John Wiley and Sons, Inc., 1963.

A-3. USA FED-INTOR 182-1, "U.S. Contribution to the International Tokamak Reactor Phase-2A Workshop", Vol. 1, 1982.

A-4. "An Analytical and Experimental Study on Lifetime Predictions for Fusion Reactor First walls and Divertor Plates", by T. Horie et al., Presented at the IAEA-TCM on Lifetime Predictions for the First wall and Bloanket Structure of Fusion Reactors, Karlsruhe, 5-7 Nov., 1985.

A-5. "Fusion Component Lifetime Analysis", by R.F. Mattas, ANL/EPP/TM-160, 1982.

A-6. "First Wall Erosion During a Plasma Disruption in Tokamak", by H. Nakamura et al, JAERI-M 83-058, March, 1983.

A-7. "Fusion Ergineering Device Design Description", C.A. Flanagan, D. Steiner, G.E. Smith, eds., ORNL/TM-7948/V2, Oak Ridge National Laboratory, December 1981.

A-8. "Thermophysical Properties of Mixed Oxide Fuel, and Stainless Steel Type 316 for use in Transition Phase Analysis", by T.C. Chawla et al, Nuclear Engineering and Design, 67, 1981, pp.57-74.

A-9. "An Assessment of Carbon and Silicon Carbide as First Wall Materials in Inertial Confinement Fusion Reactors", by G.R. Hopkins et al, GA-A14979, 1978.

A-10. "Refractory Metal Alloys for Fusion Reactor Applications", by R.E. Cold and D.L. Harrod, Journal of Nuclear Materials, 85&86, 1979.

A-11. "Blanket Comparison and Selection Study Final Report", ANL/FPP-84-1, Vol. 2, Sept. 1984.

A-12. Handbook of Chemistry and Physics, eds. R.C. Weast and M.J. Astle, 63rd Edition, CRC Press, Inc., 1982.

A-13. "ASME Boiler and Pressure Vessel Code", ANSI/ASME BPV-III-1-NB, 1977 Edition.

A-14. Private Communication with F.W. Wiffen, Oak Ridge National Laboratory, Oak Ridge, Tennessee.

A-15. "Starfire - A Commencial Tokamak Power Plant", ANL/FPP-80-1, September, 1980.

A-16. Private communication between J.R. Haines and T. Kobayashi, JAERI.

A-17. "JSME Data Book: Fatigue of Metals, IV, Low Cycle Fatigue Strength", H. Ouchida et al., eds., 1983.

Table A-1 Thermal Properties

PROPERTY	Be	Graphnol N3M	IG-110 Graphite (UNIRRADIATED)	IG-110 Graphite (IRRADIATED)	SiC	316 SS	HT-9	V-15Cr-5Ti	OFHC Cu	Cu Alloy C-17510	Mo Alloy TZM	Ta	W
Density (Mg/m^3)	1.85	1.74	1.75	1.75	3.20	7.95	7.80	6.16	8.96	8.83	10.22	16.6	19.3
Specific Heat (J/kg-K) $=C_0+C_1T(K)+C_2T(K)^2+C_3 \exp(-T(K)/C^4)$													
C_0	1210	2100	2100	2100	1500	463	530	394	386	386	220	139	128
C_1	1.34	—	—	—	—	0.134	-0.616	0.22	—	—	0.075	0.0176	0.0249
C_2	—	—	—	—	—	—	1.17×10^{-3}	—	—	—	—	1.375×10^{-6}	1.43×10^{-6}
C_3	—	-2292	-2292	-2292	-1500	—	—	—	—	—	—	—	—
C_4	—	600	600	600	487	—	—	—	—	—	—	—	—
Thermal Conductivity (W/m-K) $=K_0+K_1T(K)+K_2T(K)^2+K_3 \exp(-T(K)/K_4)$													
K_0	70	50	36	20	0	9.248	23.5	17.66	366	132.5	118	52.3	103
K_1	—	—	—	—	—	0.0157	0.0046	0.0135	—	0.310	-0.01	0.0203	—
K_2	—	—	—	—	—	—	—	—	—	—	—	-3.01×10^{-6}	—
K_3	200	294	280	—	86	—	—	—	—	—	—	—	103
K_4	370	480	278	—	1040	—	—	—	—	—	—	—	550
Melting Temperature	1557	—	—	—	2973 (decomp.)	1700	1693	2161	1356	1356	2883*	3269	3683
Latent Heat of Fusion (MJ/kg)	1.083	—	—	—	—	0.270	0.270*	0.410	—	—	0.290*	0.16	0.184
Latent Heat of Vaporization (MJ/kg)	24.8	59.1	59.1	59.1	13.1	7.27	7.27*	8.87	—	—	6.18*	4.32	4.815
Saturation Pressure (Pa) $=\exp(-A_1/T(K)+A_2)$													
A_1	3.643×10^4	8.85×10^4	8.85×10^4	8.85×10^4	6.22×10^4	4.345×10^4	$4.345\times10^{4*}$	5.89×10^4	—	—	$7.18\times10^{4*}$	1.008×10^5	9.275×10^4
A_2	24.75	32.1	32.1	32.1	23.0	25.6	25.6	27.9	—	—	26.08*	29.80	19.50
Liquid Density (Mg/m^3)	1.69	—	—	—	3.20*	6.50	6.50*	6.160*	—	—	9.62*	15	17.6
Liquid Specific Heat (J/kg-K)	3590	—	—	—	1500*	770	770*	870*	—	—	423*	180	193
Liquid Thermal Conductivity (W/m-K)	70	—	—	—	4.0*	20	20	46.8*	—	—	80*	86*	100*
Nuclear Heating Rate (MW/m^3 per 1 MW/m^2 Neutron Wall Loading)	7.8	7.0	7.0	7.0	10	10	10	7.8	14.7	14.7	13.4	19	23.3

* Estimated Value

Table A-2 Structural Properties

PROPERTY	Be	Graphnol N3M	IG-110 Graphite (UNIRRADIATED)	IG-110 Graphite (IRRADIATED)	SiC	316 SS	HT-9	V-15Cr-5Ti	OFHC Cu	Cu Alloy C17510	Mo Alloy TZM	Ta	W
Thermal Expansion Coefficient (10^{-6} K^{-1})= $\alpha_0+\alpha_1 T(K)+\alpha_2 T(K)^2$													
α_0	8.65	4.1	3.8	4.3	4.9	16.7	8.4	8.3	18	18	5.2	6.5	4.3
α_1	0.0095	1.6×10^{-3}	1.07×10^{-3}	1.07×10^{-3}	—	—	0.0044	2.5×10^{-3}	—	—	—	3.4×10^{-4}	—
α_2	—	—	—	—	—	—	—	—	—	—	—	1.2×10^{-7}	—
Elastic Modulus (GPa $=E_0+E_1T(K)+E_2T(K)^2$													
E_0	376	6.7	10	15	448	196	226	140	113	135	320	169	412
E_1	-0.243	-1.83×10^{-4}	—	—	-0.06	—	-0.096	0.0323	—	—	-0.044	-8.22×10^{-3}	—
E_2	—	9.71×10^{-7}	—	—	—	—	—	—	—	—	—	-1.66×10^{-6}	—
Ultimate Tensile Strength (MPa)	280	50	26.5	26.5*	360	510	700	600	216	827	800	180	784
Tensile Yield Strength(MPa)	200	—	—	—	—	206	500	400	68.6	758	700	45	490
Poisson's Ratio	0.06	0.2	0.15	0.15	0.24	0.3	0.27	0.3	0.33	0.33	0.29	0.35	0.28
Material Parameters for Simplified Elastic-Plastic Analysis:													
m	1.7*	1.1*	—	—	1.1*	1.7	1.7*	1.7*	1.7*	1.7*	1.7*	1.7*	1.7*
n	0.3*	0.1*	—	—	0.1*	0.3	0.3*	0.3*	0.44*	0.44*	0.3*	0.44*	0.3*
Fatigue Lifetime Limits $E_f=A\,N_f^{-a}+B\,N_f^{-b}$													
A	0.012	0.0105	—	—	—	0.70	0.80	1.78	1.758	0.0476	0.067	0.0175	1.41
a	-0.12	-0.12	—	—	—	-0.50	-0.708	-0.6	-0.7	-0 191	-0.35	-0.184	-0.62
B	—	—	—	—	—	0.012	0.0171	0.0407	0.0075	—	—	—	0.0204
b	—	—	—	—	—	-0.12	-0.116	-0.12	-0.1	—	—	—	-0.053
References	A-2,3,5	A-3,5,6,7	A-16	A-16	A-6,9	A-4,7,8,13	A-11,17	A-3,12	A-1,4,5	A-14	A-1,6,15	A-1,2,3, 5,10	A-1,2, 4,5

*Estimated value

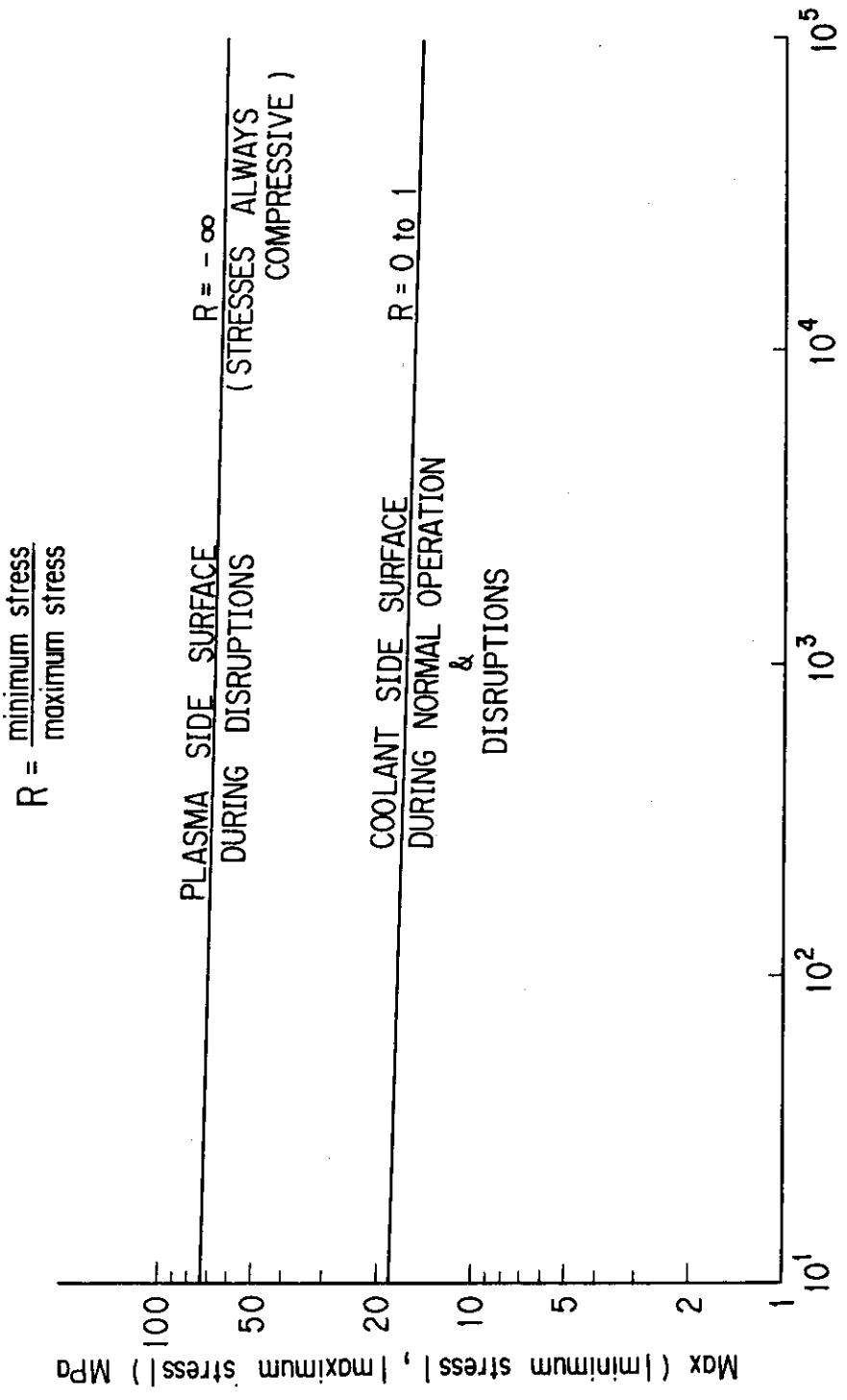

Fig. A-1 Fatigue data for IG-110 (95% confidence of 99% survival)

Appendix B. Thermal and Structural Models

Thermal Model

A one-dimensional, finite difference thermal analysis model was used for this study. The model includes:

(1) Conduction heat transfer within the structure
(2) Convection heat transfer to the coolant
(3) Radiation heat transfer from the plasma facing surface to other plasma chamber surfaces.
(4) Contact conductance and/or radiation heat transfer from the armor to the heat sink
(5) Vaporization of the heated surface, thus leading to a moving boundary problem
(6) Melting of the heated surface material, leading to an additional moving phase boundary.

A sketch of the model geometry is shown in Figure B-1. Temperature nodes are spaced, not necessarily in equal increments, throughout the armor and heat sink material. The heat diffusion equation with a volumetric heat source is solved at each internal node for each time increment using temperature dependent thermal properties. The heat diffusion equation for the heat sink material is:

$$\frac{\partial}{\partial x} k \frac{\partial T}{\partial x} + \dot{q}''' = \rho c \frac{\partial T}{\partial \tau}$$

where: T = temperature
x = distance from heated surface
τ = time
k = thermal conductivity
$\dot{q}'''$ = volumetric heating rate
ρ = density
c = specific heat.

The boundary condition at the coolant interface is simply:

$$h(T_w - T_c) = -k \left.\frac{\partial T}{\partial x}\right|_w$$

where: h = convection heat transfer coefficient
$()_W$ = value of the parameter () at the wall ($x=t+t_2$)

T_c = bulk coolant temperature

The condition at the interface between the armor and heat sink is:

$$\sigma F_e (T_1^4 - T_2^4) + C(T_1 - T_2) = -k \left.\frac{\partial T}{\partial x}\right|_{x=t_1+} = k \left.\frac{\partial T}{\partial x}\right|_{x=t_1-}$$

where: σ = Stefan-Boltzmann Constant (5.67×10^{-8} W/m^2·k^4)

F_e = emittance factor = $(1/\varepsilon_A + 1/\varepsilon_{HS} - 1)^{-1}$

ε_A = emittance of armor material

ε_{HS} = emittance of heat sink material

T_1 = Temperature of armor at armor/heat sink interface

T_2 = Temperature of heat sink at armor/heat sink interface

C = thermal contact conductance between the armor and heat sink

As shown in Figure B-2, the surface facing the plasma recedes as vaporization occurs. At this surface, the energy balance between heat input to the surface from the plasma and heat removal by radiation, conduction, and vaporization is:

$$\sigma F_A E(T_o^4 - T_s^4) + k \left.\frac{\partial T}{\partial x}\right|_{x=X} + \rho L_V \frac{dX}{d\tau} = \dot{q}_s$$

where: F_A = area view factor

E = emittance of the surface

T_o = temperature of the surface at x=X

T_s = temperature of surrounding surfaces viewed by the heated surface

X = x location of the surface as it recedes

L_V = latent heat of vaporization

$\dot{q}_s$ = surface heat Flux

The surface recession rate $\left(\frac{dX}{d\tau}\right)$ is given by:

$$\frac{dX}{d\tau} = J\,\hat{\rho}$$

where $\hat{\rho}$ is the atomic density of the material undergoing evaporation and J is the net flux of atoms leaving the surface. For evaporation into a vacuum, the flux of atoms leaving the surface (J_v), assuming that the vapor is completely removed from the surface (i.e. no recondensation), is simply:

$$J_v = (2\pi m\, k_B T_o)^{-\frac{1}{2}}\, P_s(T)$$

where: m = moleculur weight
k_B = Boltzmann constant (1.38×10^{-23} J/K)
$P_s(T)$ = the temperature dependent saturation pressure

For the intense evaporation conditions experienced during a plasma disruption, the finite vapor density in the surface region may affect the net flux of atoms. The model employed by Hassenein[B-1], which is based on results of transport calculations for intense evaporation[B-2], is used in this study. According to this model the net evaporation is:

$$J = J_v\, [0.8 + 0.2 \exp\, (-\tau_V/\tau_R)]$$

where: τ_V = time from start of intense evaporation
τ_R = relaxation time = $(2.735\, \hat{\rho}^{2/3}\, J_V)^{-1}$

To model the moving evaporation boundary, a moving coordinate system $\eta(\tau)$ is introduced:

$$\eta(\tau) = x - X(\tau)$$

This moving coordinate system leads to a convective term in the heat diffusion equation for the plasma facing material. The geometry of an elementary volume (i.e. elementary length for this one-dimensional case) in this coordinate system is shown in Figure B-3. The energy balance for this elementary volume defined by a width $d\eta$ is:

Energy increase in $d\eta$ = Heat Conducted into $d\eta$
- Heat Conducted out of $d\eta$ + Volumetric heating in $d\eta$
+ Energy in region C
- Energy in region A

$$\rho c \frac{\partial T}{\partial \tau}\, d\eta = k \left.\frac{\partial T}{\partial \eta}\right|_{x_1} - k \left.\frac{\partial T}{\partial \eta}\right|_{x_1 + d\eta} + \dot{q}'''\, d\eta + \frac{\partial}{\partial \tau}\, (E_c - E_A)$$

The thermal energy in regions A and C are:

$$E_A = \rho \frac{[h(x_0) + h(x_1)]}{2} d\eta$$

$$E_C = \rho \frac{[h(x_0+d\eta) + h(x_1+d\eta)]}{2} d\eta$$

where h is the enthalpy.
Expanding the values for $h(x_1)$, $h(x_0+d\eta)$, and $h(x_1+dn)$ in Taylor series about x_0 neglecting higher order terms we obtain:

$$E_A = \rho \left[h(x_0) + \frac{dh}{d\eta}\bigg|_{x_0} \frac{\Delta x}{2} \right] d\eta$$

$$E_C = \rho \left[h(x_0) + \frac{dh}{d\eta}_{x_0} d\eta + \frac{dh}{\partial\eta}\bigg|_{x_0} \frac{\Delta x}{2} \right] d\eta$$

Thus the convective term becomes:

$$\frac{d}{d\tau}(E_C - E_A) = \rho\, d\eta \frac{d}{d\tau}\left(\frac{dh}{d\eta}\bigg|_{x_0} d\eta\right) = \rho\, d\eta \frac{dh}{d\eta}\frac{d\eta}{d\tau} = -\rho c\, d\eta \frac{\partial T}{\partial \eta}\frac{d\eta}{d\tau}$$

Recalling that $\eta(\tau) = x - X(\tau)$, we obtain:

$$\frac{d}{d\tau}(E_C - E_A) = \rho c \frac{\partial T}{\partial \eta}\frac{dX}{d\tau} d\eta$$

Substituting this result, and also the result obtained by expanding the conduction term in a Taylor series and simplifying, into the heat balance yields the heat diffusion equation for the armor material:

$$\rho c \frac{\partial T}{\partial \tau} = \frac{\partial}{\partial \eta} K \frac{\partial T}{\partial \eta} + \dot{q}''' + \rho c \frac{\partial T}{\partial \eta}\frac{dX}{d\tau}$$

The melting process is modeled by artificially increasing the specific heat over a narrow range of temperature (ΔT_m), for example 20 °C, bracketing the melting temperature. This increased specific heat C_{eff} is:

$$C_{eff} = C + \frac{L_f}{\Delta T_m}$$

where L_f is the latent heat of fusion.

The finite difference scheme used in this model is backward difference in time and mid-difference in the spatial coordinate.

Node sizes near the surface were typically about 2 μm thick for the intense disruption heating analysis and 0.5 mm for the analysis of normal operating conditions. Node sizes were increased with distance from the heated surface. The total number of nodes in the plasma facing material was usually 30 (about 10 for normal operation) and about 10 in the compliant layer and heat sink materials.

Stress Model

The temperatures predicted using the thermal model were used to predict the thermal stress distribution in the first wall and divertor plate structures. The one-dimensional, elastic model used in this study determines the stresses and strains for three types of constraint conditions. These constraint conditions are shown schematically in Figure B-4. Free expansion allows the plate to expand laterally and to bend. If properties are constant and a linear temperature distribution exists, the thermal stresses will be zero for this constraint condition. However, for our case properties vary through the thickness due to temperature dependence as well as the use of different heat sink and armor materials. A non-limear temperature distribution is also caused by the volumetric heating from neutron interactions with the materials. Therefore, eren for the free expansion case, we expect significant stresses. For a fully constrained design, the stresses are maximum and always compressive (for heating). The constraint which appears most realistic in modeling an actual first wall or divertor plate design is expansion with no bending. Results with this intermediate constraint were shown to match well with those of two and three dimensional results from previous analyses of FER first wall and divertor designs. This is not surprising, since these desings consist of relatively thin plasma facing structures attached to solid support structures (e.g. first wall is attached to thick shield structure. Results presented in this study are for the expansion but no bending constraint condition. Therefore, only this case is discussed below.

For a plate that expands a uniform amount laterally, i.e. no bending, the strain (ε) at a given location through the plate is simply the difference between the thermal expansion of the plate element ($\alpha\Delta T$) and the uniform expansion ($\bar{\varepsilon}$) of the entire plate thickness:

$$\varepsilon = \bar{\varepsilon} - \alpha\Delta T$$

where: α = thermal expansion coefficient

ΔT = temperature rise from initial value at zero stress

The resulting stresses (σ_y and σ_z) parallel to the y and z directions are:

$$\sigma_y = \sigma_z = \frac{E(\bar{\varepsilon} - \alpha\Delta T)}{1 - \nu}$$

where: E = elastic modulus

ν = poissons ratio

The condition of equilibrium is:

$$\int_0^t \sigma_y \, dx = \int_0^t \sigma_z \, dx = 0$$

where: t = thickness of structure. Substituting the equations for stress into the equilibrium condition yields:

$$\bar{\varepsilon} = \frac{\int_0^t \frac{E\alpha\Delta T}{1-\nu} \, dx}{\int_0^t \frac{E}{1-\nu} \, dx}$$

Therefore, the stress at anylocation is:

$$\sigma_y = \sigma_z = \frac{E}{1-\nu}\left[-\alpha\Delta T + \frac{\int_0^t \frac{E\alpha\Delta T}{1-\nu} \, dx}{\int_0^t \frac{E}{1-\nu} \, dx}\right]$$

The primary stress caused by the coolant pressure is not included in this study. It should be simple to limit these stresses to acceptable levels. The secondary cyclic thermal stresses are caused by thermal strains. Thus, strain limited fatigue data were used for the fatigue lifetime evaluation.

Since the thermal stresses can be allowed to exceed the elastic limit, plastic effects must be included in the analysis. For a parametric study over a broad range of conditions and materials, sophisticated analysis methods, such as that described in Ref. B-3,

were judged to be too time consuming and expensive. The simple elastic plastic model describes in the ASME-Boiler and Pressure Vessel Code[B-4] was applied. For this procedure, stresses are first calculated using an elastic model, such as that described above. The values of stresses (or strains) calculated elastically are then multiplied by the factor Ke before entering the design fatigue curve. The factor Ke depends the elastically calculated stress (Sn) as follows:

$$Ke = 1.0 \text{ for } Sn < 3\ Sm$$

$$= 1.0 + \frac{(1-n)}{n(m-1)}\left(\frac{sn}{3\ Sm} - 1\right) \text{ for } 3\ Sm < Sn < 3m\ Sm$$

$$= 1/n \text{ for } Sn \geq 3m\ Sm$$

where Sm is the lower of one-third the ultimate strength or 2/3 the yield strength.

This simple procedure for calculating the stresses elastically and then converting these results to equivalent plastic stresses was shown in previous FER studies to be quite conservative. Results should be treated as yielding a reasonably good qualitative comparison between design concepts and materials but only a rough estimate of the actual fatigue lifetime.

References

B-1. A.M. Hassenein, et al., J. Nucl. Mater. 111 & 112 (1982).

B-2. S.I. Anisimor, et al., Sov. Phys. JETP 37 (1973).

B-3. T. Horie et al., "An Analytical and Experimental Study on Lifetime Predictions for Fusion Reactor First Walls and Divertor Plates", Presented at the IAEA-TCM on Lifetime Predictions for the First Wall and Blanket Structure of Fusion Reactors, Karlsruhe, FRG (1985).

B-4. ASME Boiler and Pressure Vessel Code, ANSI/ASME BPV-III-1-NB, Nuclear Power Plant Components (1977).

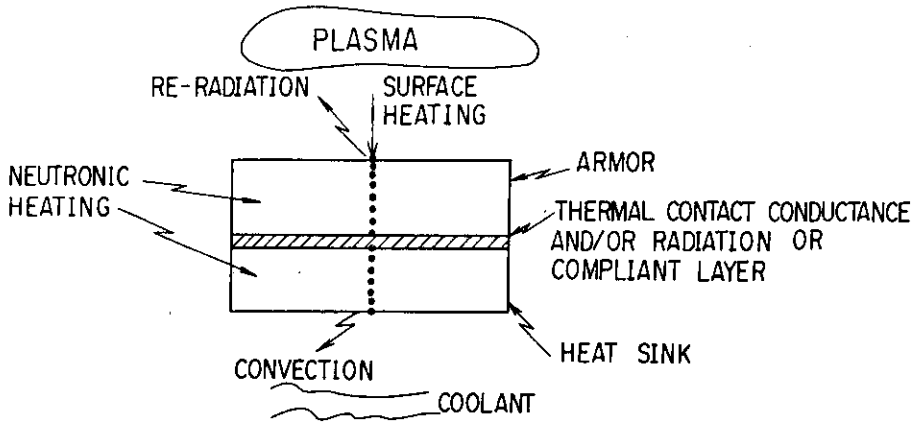

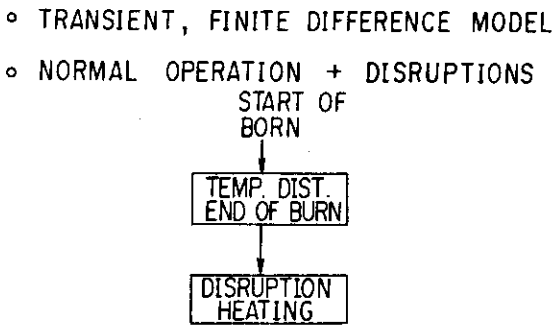

Fig. B-1 1-D thermal model

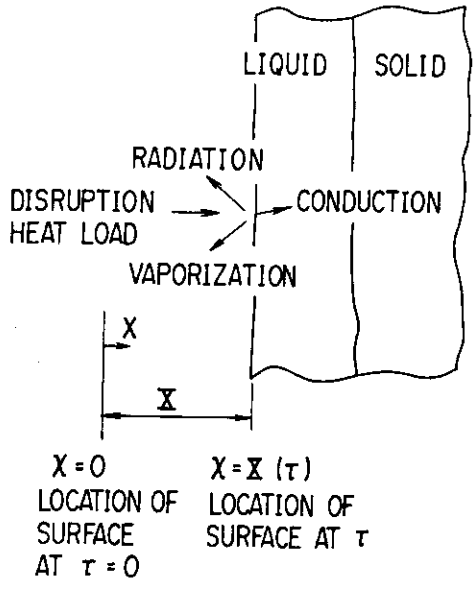

Fig. B-2 Geometry for disruption vaporization and melting model

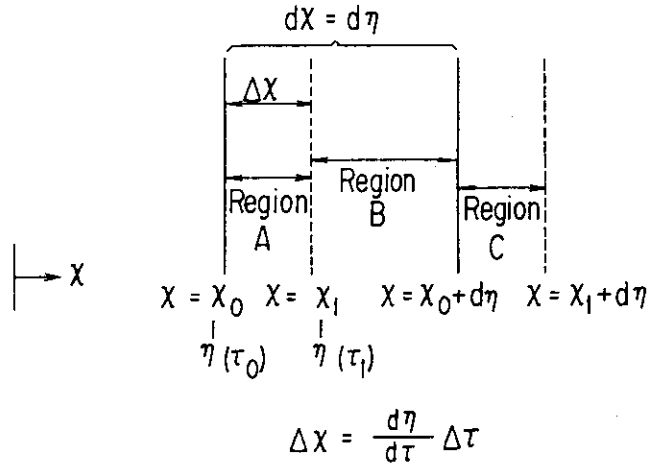

Fig. B-3 Elementary volume

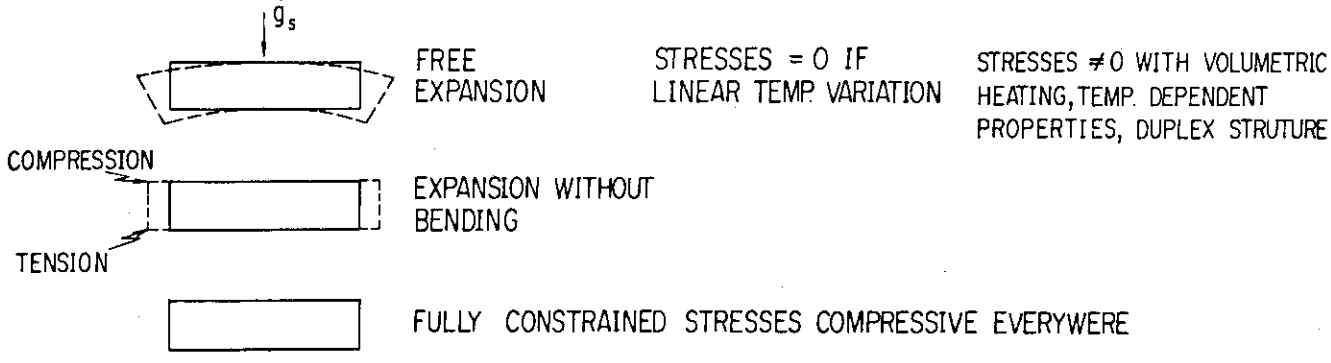

Fig. B-4 Constraint conditions for the 1-D thermal stress model